Novel Micropatterned Substrate for Investigation of Ovarian Cancer Aggregate Formation and Response to Epigenetic Drug Therapy

by
Fatima Alshamsi

A thesis submitted to the Department of Engineering Technology,
College of Technology
in partial fulfillment of the requirements for the degree of

Master of Science
in Engineering Technology

Co-Chair of Committee: Dr. Fatima A. Merchant, Professor, University of Houston

Co-Chair of Committee: Dr. Venkatesh Balan, Assistant Professor, University of Houston

Committee Member: Dr. Wanda Wosik, Associate Professor, University of Houston

University of Houston
December 2020

ACKNOWLEDGMENTS

First of all, I would like to express my deepest appreciation to my advisor, Dr. Fatima A. Merchant, for all of her help and support throughout my undergraduate and graduate years at the University of Houston. Dr. Merchant not only has she helped me become a better researcher, but also her dedication to research and teaching has been a source of inspiration for me. Working in her lab was one of the best things that have ever happened in my life, which changed my path forever. I would also like to thank Dr. Balan, not just for all that I learned throughout his courses as a Biotechnology student, which helped me in completing this degree, but also for helping me work on my presentation skills, improve my article reviews, and understand the overall work that goes behind every published paper. Thank you, Dr. Wosik, for creating such a multifaceted platform that has made all this possible and for serving on my thesis committee. Furthermore, I had the pleasure of working with Dr. Lewis Francis from Swansea University, who provided me with priceless knowledge and experience. Additionally, I would like to appreciate the help of Jefferson Friguglietti and Darius McPhail in conducting this research. I would also like to thank my friends and colleagues in the Ovarian Cancer Research Lab, Phi Le, Margaret Eisenbrandt, and Luis Segura, for their help along the way. Also, I would like to thank my partner for all of her tremendous support over these years and for being a constant source of positivity to endure all the difficulties of being this far away from my home. Lastly, I would like to thank my childhood mentors who have always supported me. They were a constant source of motivation. None of this would have been possible without you all; your insights and your encouragements.

ABSTRACT

Ovarian Cancer (OvCa) is the deadliest gynecological cancer, with 90% of mortality being a direct result of metastasis. At this late stage, ovarian cancer is more challenging to treat, with only approximately 20% of women at an advanced-stage surviving beyond 12 years after treatment. Tumorigenesis is complex, and the heterogeneity of most tumors further exacerbates attempts for developing therapeutics. Several factors play a role in the elucidation of processes, one of which is the cellular microenvironment. The current consensus in cancer research is that 3D microenvironments are needed to better mimic *in vivo* response of tumors to drugs. This study will evaluate the feasibility of using a novel micropatterned substrate that enables 3D microenvironments for *in vitro* investigations of OvCa. The substrate was created through technologies used in integrated circuit fabrication utilizing micropatterns of titanium diboride etched on a silicon wafer (Si-TiB_2). TiB_2 micropatterns on the Si background establish stiffness, roughness, wetness, and charge gradients to induce selective deposition of growth factors, enabling self-assembly of cells into 3D aggregates. OVCAR3 and SKOV3 cell lines were used in the absence/presence of pan-genome epigenetic drugs such as suberoylanilide hydroxamic acid (SAHA). The micropatterned substrate supported cell proliferation, migration, and aggregate formation while maintaining phenotype and viability. Treating aggregates with SAHA maintained cell viability but caused disaggregation of SKOV3 aggregates. The micropatterned substrate allows investigations of drug therapy for cancer treatment. Furthermore, results suggest that epigenetic treatments have potential use for OvCa treatment.

TABLE OF CONTENTS

LIST OF FIGURES

CHAPTER 1 INTRODUCTION

1.1 Motivation

A collective term for distinct diseases of different etiology, biomarker expression, and prognosis, Ovarian Cancer (OvCa) ranks fifth in the causes of cancer-related deaths among women. The most common OvCa subtype is epithelial, which accounts for 90% of all cases, and its invasive and malignant form accounts for 70% of all OvCa cases (Fig. 1.1) [1,2]. Interestingly, recent research suggests that most OvCa often originates in other organs, such as the fallopian tube, endometrium, gastrointestinal tract, endocervix, or urinary bladder. Intra-abdominal dissemination is particularly prevalent in epithelial ovarian cancer (Fig. 1). Metastatic cells often disseminate and grow in the intra-abdominal space in gastrointestinal (GI) and gynecological cancers. Moreover, it is sometimes difficult to differentiate ovarian carcinomas from tumors of the GI tract [15–17,20].

There's a number of genetic, physiological, and lifestyle-related factors that have been considered to play an etiologic role in OvCa. The main genetic factors include epigenetic silencing, heritable, or somatic mutations of DNA repair proteins, such as CDK12, and DNA copy number. Other genetic factors include mutations in the BRCA1 and BRCA2 genes, as well as the genes related to other cancer syndromes linked to an increased risk of ovarian cancer, such as PTEN (tumor hamartoma syndrome), STK11 (Peutz-Jeghers syndrome), MUTYH (MUTYH-associated polyposis and colon cancer) [21–23]. Moreover, different alterations of cytokines and chemokines as well disturbances of the hormonal environment during reproductive and menopausal age can

distinctively affect the phenotype of these malignant precursors, thereby potentially promoting or even promoting a specific stage in the process of OvCa origin and progression [24–26].

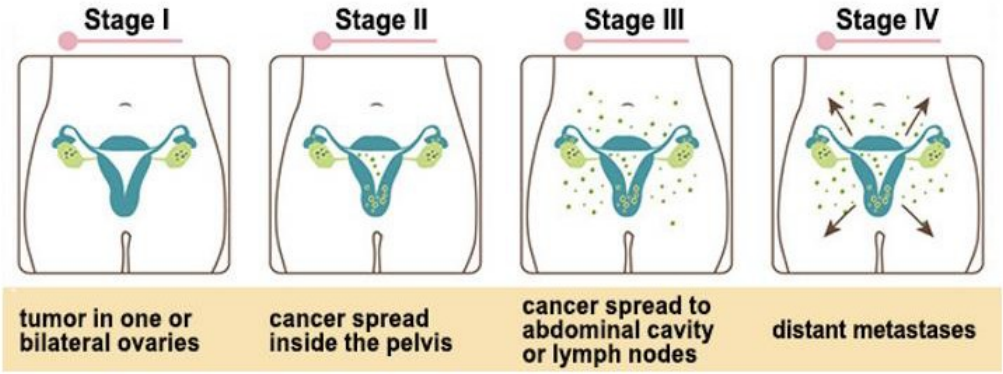

OVARIAN CANCER
survival rates

	Invasive epithelial ovarian cancer	Ovarian stromal tumors	Ovarian germ cell tumors	Fallopian tube carcinoma
Stage 1	90%	95%	98%	87%
Stage 2	70%	78%	94%	86%
Stage 3	39%	65%	87%	52%
Stage 4	17%	35%	69%	40%

Figure 1.1: (A) Staging of OvCa according to the size of the primary tumor, and the extent the disease has spread to other locations. The stage at diagnosis can greatly affect prognosis – National Ovarian Cancer Coalition. (B) The 5-year survival rate for various types of ovarian cancer – American Cancer Society, Healthline. The average 5-year survival rate for all the mentioned types is 45%. [Figure taken from the National Ovarian Cancer Coalition, the American Cancer Society, and Healthline [1,2]].

With a prevalence of 1 in 2,500 in post-menopausal women, OvCa presents an exceptionally high mortality rate across all types (Fig. 1.2A). As of this year, annually over two hundred and ninety-five thousand women are diagnosed with ovarian cancer, most of which are at Stage III of the disease's progression. What's even more astounding is that these numbers are predicted to increase by 55% with the number of deaths rising to 70% (Fig. 1.2B). This means hundreds of thousands of annual deaths are caused by this one form of cancer [1,3,27]. The grim outlook for patients is partly due in part to the heterogeneity of the disease, the lack of sensitive screening test to detect early stages of the disease, and the fact that 75% of cases are not presented until cancer has metastasized [28,29].

Early OvCa is often symptom-free. Moreover, although routine pelvic exams, such as a pap smear, can be useful in finding some gynecologic cancers at an early stage, in most cases early ovarian tumors are difficult or impossible to detect via these methods due to the relative inaccessibility of the ovaries. This often leads to a delay in the detection of borderline tumors and other ovarian malignancies[30].

Moreover, the American Cancer Society and the American College of Obstetrician and Gynecologists (ACOG) do not recommend screening for ovarian cancer in average-risk women due to the lack of established identifiable histologic precursor lesions or molecular events that precede malignant transformation and the fact that risks and harms outweigh the benefits [31]. As of now, the search for an ideal screening test for OvCa has been ongoing.

Transvaginal ultrasound (TVUS), Carcinoma Antigen (CA)-125 blood tests, and bimanual pelvic examination have been used in various studies to evaluate their role as

screening tests, however, they have not found much supportive evidence as far as accuracy or sensitivity [21,27,30,31].

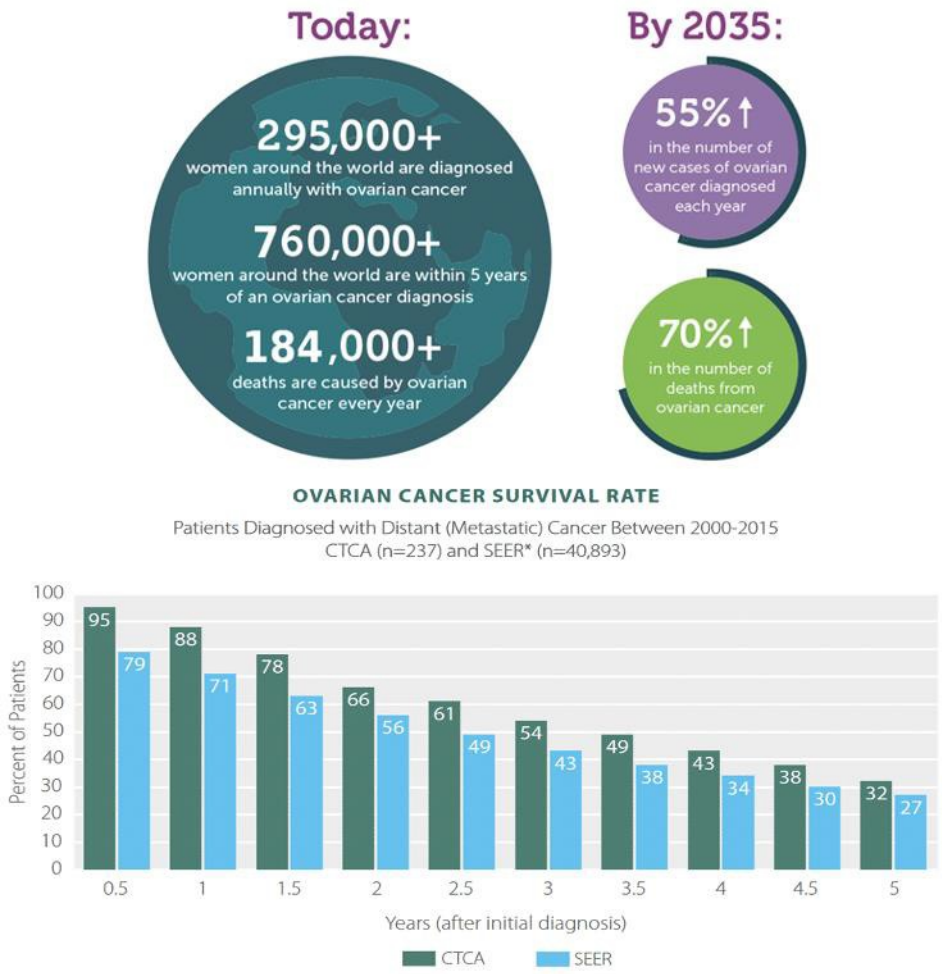

Figure 1.2: (A) Statistics of Ovarian Cancer from Today to the year 2035. International Federation of Gynecology & Obstetrics – World Ovarian Cancer Coalition – WOCD Statistics. (B) CTCA and SEER survival rates for ovarian cancer patients with the distant (metastatic) disease who were diagnosed between 2000 and 2015. CTCA data comes from the Cancer Treatment Centers of America. While SEER data represent national results over a large number of institutions. [Figures taken from the World Ovarian Cancer Coalition, Cancer Treatment Centers of America, the National Cancer Institute's Surveillance, Epidemiology, and End Results (SEER) Program database, and the National Cancer Database (NCDB) [3,4]].

TVUS screens by using sound waves to look at the uterus, fallopian tubes, and ovaries. It can help find a mass in the ovary, but it can't determine if a mass is malignant or benign. When it is used for screening, most of the masses found are benign, which

has led to greater unnecessary surgeries. On the other hand, CA-125 blood tests screen for a mucin glycoprotein that is known to enable tumor cell growth, promote cell motility, and facilitate invasion through its selective mesothelial binding and induction of cell-cell interaction in tumorigenesis. Although CA-125 tests have been seen as useful tumor markers in women known to have ovarian cancer, because a high level often goes down if treatment is working, high levels of CA-125 are more often caused by common conditions such as endometriosis and pelvic inflammatory disease. Moreover, not everyone with ovarian cancer has elevated CA-125 levels; thus false positives are more common, which leads to a cycle of more tests [32,33].

Currently, there are essentially two treatment approaches for OvCa: Local or Systemic. Local treatments attempt to address the tumor with minimal effect to the rest of the body, while systemic treatments aim to reach cancer cells regardless of their location and address more symptoms. The most commonly advised therapeutic option to treat patients with OvCa involves surgically removing as much of the tumor as possible, followed by treatment with adjuvant platinum or taxane-based therapy, often utilizing Cisplatin and Paclitaxel [32,34]. Surgery often means seeing how far cancer has spread and removing what is necessary; how much surgery you have also depended on how your general health is. If your tumor isn't properly excised, you may need to have more surgery in the future. Chemotherapy can be useful to kill very small amounts of cancer cells that may still be around after surgery, in the case of post-metastasis tumors, or to shrink very large tumors to make surgery easier. Most of the time, chemotherapy uses drugs that are injected intravenously; however, in some cases an intraperitoneal catheter is used [35–38].

Four decades' worth of studies and clinical experiments suggested that combination chemotherapy with platinum/taxane should be accepted as the standard regimen in advanced ovarian cancer with several randomized clinical trials demonstrating a survival advantage for advanced-stage patients. Alternatively, the development of differential subtype and stage-specific treatment shows the greatest potential at improving survival rates, especially as different subtypes have been shown to exhibit varying responses to chemotherapy. Many possible new treatment options are emerging from recent clinical trials, based both on the modifications of standard approaches and on the addition of new biological drugs to the standard treatment [39,40].

There is an ongoing debate whether single or multi-agent therapy is more beneficial, however, combination therapy of drugs and other small molecules demonstrates the greatest potential through enhancing the therapeutic efficacy of platinum/taxane-based chemotherapy by increasing drug sensitivity and reducing resistance. For example, the combination of platinum drugs with bortezomib, a modulator for copper transporter expression, is a current option for platinum-resistant solid tumors with promising outcomes. Moreover, compelling data is emerging to show that a combinational approach in preclinical studies shows induction of immune signaling [41,42].

In-line with studies covering other cancer types, future advanced treatments could arise from cancer immunotherapy, smart drug delivery systems, epigenetic drugs, and the combination of these with traditional chemotherapy. Although in most studied cancer types fewer than half of patients respond to these immunotherapies, more

research needs to be conducted especially since current epigenetic therapy has been seen to alter targeted gene activity without affecting the overall DNA sequence. These drug classes have been used mainly with liquid cancers so far, but there is an urgent call to use them on solid tumors, such as OvCa, either as sensitizing agents for chemotherapy at advanced stages or in combination with chemotherapy. Excitedly, these therapies have demonstrated an ability to activate the host immune system and reduce the tumor burden, which further indicates astounding promise for a variety of solid tumors. However, in most cancer types, fewer than half of patients respond to these immunotherapies [43,44].

Despite all the research dedicated to OvCa screening and therapy, generally, 70% of advanced-stage ovarian cancer relapses, with even stage I and II patients experiencing relapse at a rate greater than 20% (Fig. 2B). The survival curve after recurrence never plateaus, with one study claiming that the post-relapse median is still 2.6 years. This means that OvCa patients, regardless of remission, still have a particularly poor prognosis, thus the goal of treatment after relapse should be controlling the disease and symptoms, limiting treatment-related toxicity or other adverse reactions, and maintaining or improving the patients' quality of life [45,46].

There has been a plethora of paradoxical data concerning chemotherapy's effect on the rate of relapse and metastasis. Due to conflicting results, physicians often hesitate to prescribe further chemotherapy to recurrent OvCa patients. A complete response to chemotherapy is rare and induced shrinkage of the tumor does not always ensure the prolongation of survival. Alternatively, a surgical approach is deemed more clinically beneficial to patients. Moreover, a less traditional perspective that seems to be gaining

popularity is the use of topoisomerase inhibitors, epigenetic treatments, and oral etoposide for platinum-resistant OvCa [36,47]. Additionally, quality of life is an increasingly important issue in patients with OvCa with most surveys strongly indicating that relapse of the disease has a profoundly negative psychological and physical impact [46] The key to improving health outcomes remains timely and accurate diagnosis, whilst highlighting the importance of time without recurrence and the need for effective long-term treatment.

Due to the high relapse rates and diverse chemo-resistant forms of OvCa, a greater understanding of the progression of the disease is needed, to allow earlier detection with specific biomarkers, as well as the discovery of new therapeutic options. Recent years have failed to see significant breakthroughs in the treatment of metastatic OvCa. Over the past hundred years, monolayer (two-dimensional (2D)) cell cultures in tissue culture flasks have been used as in vitro models to study cellular behavior in health and disease. Although conventional 2D monolayer cell cultures have greatly advanced our understanding of cell behavior, there is now growing evidence that the 2D platforms are not appropriate for cancer cells. Thus, the last few decades have seen tremendous growth in the development of in vitro 3D cell culture platforms that better mimic in vivo conditions allowing cancer cells to grow in aggregates or spheroids [48,49].

Moreover, the use of 3D culture platforms has unequivocally demonstrated that extracellular matrix (ECM) rich 3D microenvironments significantly impact cell proliferation, differentiation, mechano-responses, and cell survival [50–52]. Importantly, it is now known that the progression and spread of OvCa are affected by

ECM stiffness and mechanical forces [53–55]. Consequently, 3D culture models are finding increasing use in OvCa research. Currently, in vitro 3D culture models for cancer research include multicellular spheroids grown in suspension, and cells were grown in naturally derived extracellular matrices (ECM) or natural (collagen) and synthetic gels. However, these approaches have experimental and interactive limitations, such as difficulties with spheroid handling and batch-to-batch differences in spheroid morphology that can affect the reproducibility of experimental outcomes and limit comparative studies.

We have developed a novel substrate for in vitro 3D culture that mitigates limitations related to accessibility and handling that are inherent in conventional low attachment plate or gel-based approaches. This study will evaluate the potential of a novel micropatterned substrate created through technologies used in integrated circuit fabrication utilizing micropatterns of titanium diboride etched on a silicon wafer (Si-TiB_2), to study specific OvCa growth and response to drug therapy. TiB_2 micropatterns on the Si background establish stiffness, roughness, wetness, and charge gradients to induce selective deposition of growth factors, enabling self-assembly into 3D aggregates. This substrate has been previously validated through growing human umbilical vein endothelial cells (HUVECs) and human adult bone marrow-derived mesenchymal stem cells (MSCs) [56]. In this study, ovarian cancer cells were grown on the substrate, and monitored for proliferation, morphology, and phenotypic changes. OVCAR3 and SKOV3 ovarian cancer cell lines were used in the absence/presence of pan-genome epigenetic drug; suberoylanilide hydroxamic acid (SAHA).

1.2 Objective

The overall goal of this study is to evaluate the efficacy of the substrate for 3D culture of OvCa cells and determine its utility for monitoring the response of cancer cells to drug therapy. The specific objectives of this study are:

- Evaluating the potential of microfabricated silicon substrates with titanium diboride micropatterns for studying Ovarian Cancer aggregate formation.
- Observing the effects of substrate properties on cell proliferation and morphology.
- Investigating the expression of mesenchymal biomarkers and aggressive behavior on surfaces with varying stiffness.
- Utilizing the novel substrate to observe the effects of disturbances caused by epigenetic treatments.

CHAPTER 2 RELATED WORK

2.1 Ovarian Epithelial Cancer

There are approximately 100 publicly available ovarian cancer cell lines, however, their cellular and molecular characteristics are largely undescribed. The Ovarian Cancer Cell Line Panel (OCCP) highlights the clinical importance of understanding and characterizing the differences of the morphological subtypes via *in vitro* studies [57]. OvCa cells lines expressing traditional epithelial-like morphology are cultured from tissue and are closely adjoined by specialized membrane structures such as tight, adherent, and gap junctions, while cell lines that express a mesenchymal-like morphology are extracted from swollen compromised tissue such as in ascites or pleural effusions and form an organized cell layer.

Genomic profiles for epithelial cell lines indicate that both OVCAR3 and SKOV3 are considered chemo-resistant serous adenocarcinomas. The main differences between both cell lines are their morphologies and their different levels of invasiveness (Fig. 2.1A). OVCAR3 has a rounded shape and tends to present less invasion potential, while SKOV3 has a more spindle-like shape with greater invasion potential (Fig. 2.1B). Serous tumors commonly arise in the epithelium of the fallopian tube fimbria and subsequently present as apparent ovarian tumors after implantation in the ovary and present at an advanced stage, are fast-growing, and spread throughout the peritoneal cavity [58,59]While studies have shown the genetic mutation of OVCAR3 tumors is distinct from SKOV3 tumors, their differences in invasiveness behavior are poorly defined and thus highlight the importance of understanding how the treatment of tumors with therapeutic options might influence invasive and migratory behavior [60,61].

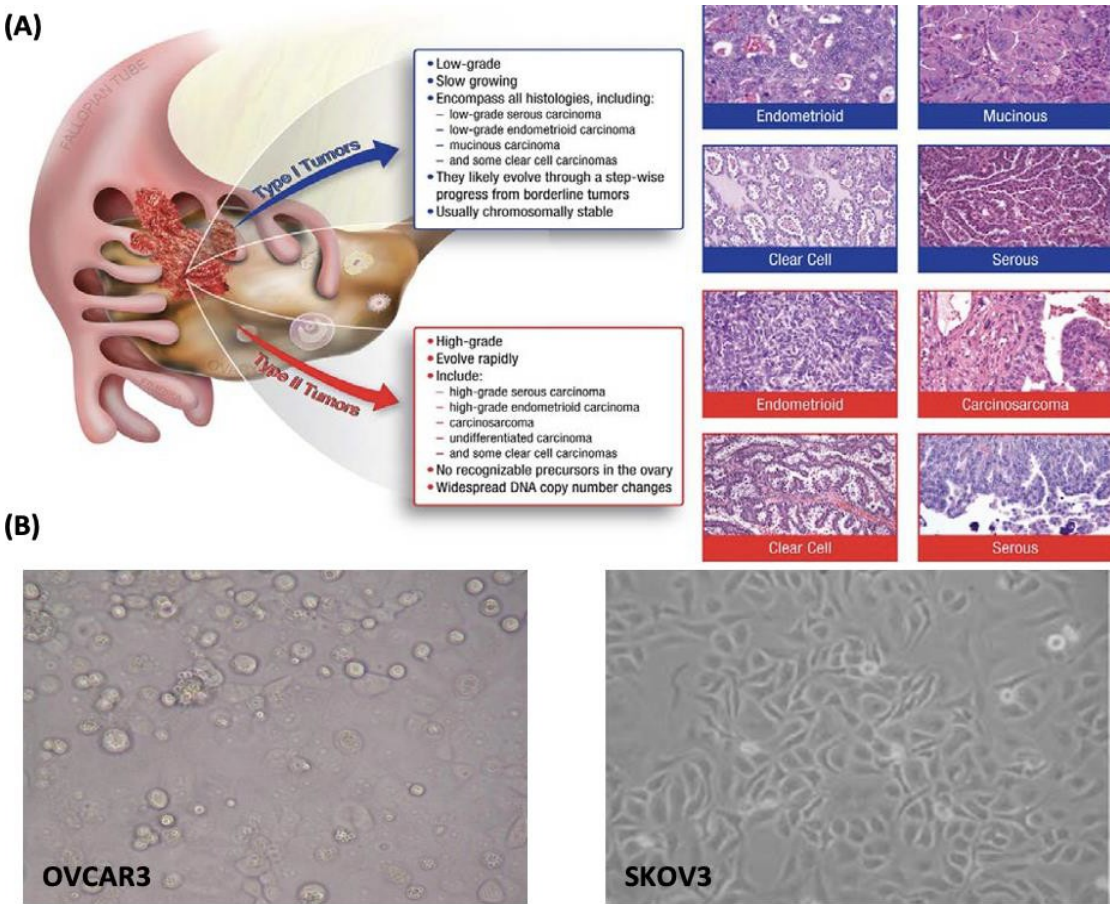

Figure 2.1: (A) Grading of OvCa by the histological presentation of the cancerous tissue compared to healthy tissue. Low-grade tumors grow slower, while high-grade ones grow faster. – National Ovarian Cancer Coalition. (B) Phase Contrast Image-Based monitoring of OVCAR3 and SKOV3, highlighting morphological aspects. [Figure taken from [4,5]].

2.2 Three-Dimensional Culture Systems

Many studies have attempted to better characterize ovarian cancer cell behaviors utilizing different techniques including two-dimensional (2D) and three-dimensional (3D) culturing. 2D cell culturing, while simple and affordable, often does not capture the true cellular arrangement of tumors *in vivo*. Also, 2D culturing often utilizes cells grown on a flat, rigid substrate, which deviates from *in vivo* tissue architecture, and can

have an overall negative impact on cellular adhesions and transcriptome profile (Fig. 4) [52,62].

Additionally, unlike 3D culturing, traditional 2D culturing does not provide the ability to promote the formation of 3D spheroids which enhances cell-cell endocrine signaling within the spheroid itself and as reported by Mitra et al. [63]. In a cross-sectional study focusing on mechanisms of metastasis of BRCA gene associated OvCa spheroids in 3D culture models, they have compared different 3D scaffolds and concluded that 3D environments create a more realistic and translational platform for studying OvCa [64].

Multicellular tumor spheroids may be formed using non-adherent culture environments such as static suspension, hanging drop method, spinner bioreactor, rotational bioreactor, magnetic levitation, microfluidic system, and gel embedding (Fig. 2.2A-D) [65,66]. Traditionally 3D spheroids can also be produced via adherent culture environments like low attachment plates and collagen/Matrigel methods. These technologies rely on creating cellular aggregates by utilizing non-adherent conditions or exposing cells to gravitational force and the shear stress of floatation. These models can capture short-term molecular changes within cells, providing a useful snapshot of the disease progression [67,68].

More recently, 3D culture techniques are a step forward, as they use engineered constructs for cell culture substrates to create a three-dimensional microenvironment. Some examples of 3D substrates available include collagen scaffolds, or hydrogels, which allow cells to grow in adherent culture environments.

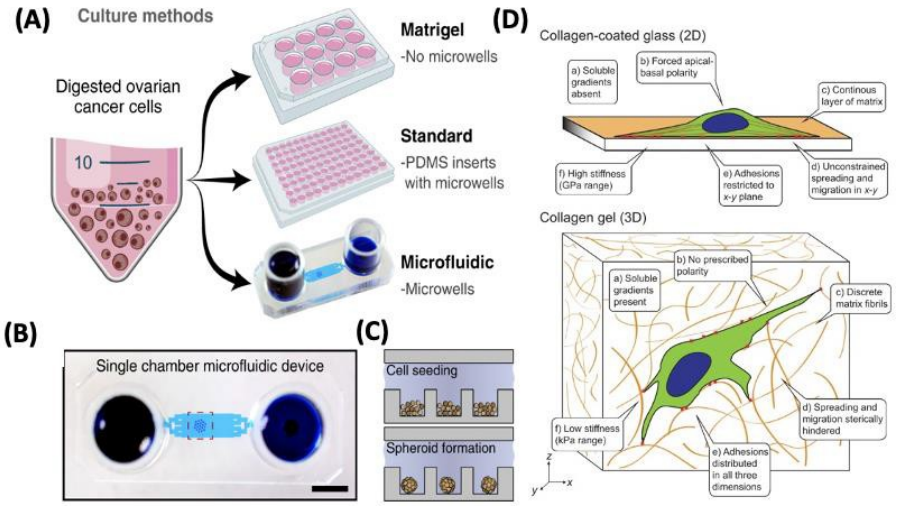

(E)

Adhesive, topographical mechanical and soluble cues in 2D and 3D

2D	3D
High stiffness surfaces provide supraphysiological mechanical signals	Tunable, relatively low stiffness environment closer to that of tissues
Continuous, flat surface available for unencumbered adhesion, spreading, and migration	Nano- and micro-scale 3D surfaces provided by ECM fibers and matrix porosity guide and hinder cell motility
Soluble gradients absent without microfluidics	Gradients of soluble factors, nutrients, and oxygen based on diffusion through gel or cell aggregates
2D geometry constrains morphogenesis and cell-substrate interactions dominate	Free to self-organize in 3D. In multicellular structures, cell-cell interactions dominate.
Automatic apical-basal polarization	Embedded cells generate apical-basal polarity on their own

Figure 2.2: (A) Culture methods for OvCa spheroids. Matrigel cultures established in 6-well plates coated with 100% Matrigel containing no microwells. Both standard and microfluidic cultures contained microwells of the same dimensions (250 μm diameter and 300 μm in depth) for spheroid formation. (B) An image of a microfluidic chamber containing an array of 19 microwells for spheroid formation. The array of spheroids was connected to media reservoirs via a transport channel. The dotted square shows the location of the microwells. Scale bar = 5 mm. (C) Schematic depicting seeding of cells and spheroid formation. (D-E) Adhesive, topographical, mechanical, and soluble cues in 2D and 3D. The cues encountered by a cell are strikingly different between an ECM-coated glass or plastic surface (2D) and a typical 3D ECM, such as collagen. [Figures taken from [6,7]].

However, low stiffness, limited long-term stability, and batch-to-batch variability limit these kinds of 3D spheroid culturing techniques [9,53,54,69]. Even with these limitations, these recent 3D culturing systems provide a unique ability to investigate the role of extracellular matrices on tumor invasiveness and behavior.

2.3 Mechanical and Chemical Gradients in Tumor Microenvironment

The role of the tumor microenvironment and the reciprocal interactions in ovarian cancer development is still a relatively new and rapidly advancing field. With better comprehension, it could present an alternative approach towards controlling growth, invasion, migration, and metastasis especially for chemo-resistant aggressive tumors [55,70]. The tumor microenvironment is a keystone of ovarian cancer progression and chemoresistance, inducing both biochemical and physical cues, promoting tumor stroma, and biomechanical abnormalities. These abnormalities derive from different factors including the tumors' extracellular matrix (ECM) and stromal cells such as cancer-associated fibroblasts (CAFs), adipocytes, and mesothelial cells (Fig. 2.3). The tumor stroma aids the progression of tumor growth through the release of various cytokines and interleukins [71,72]. Additionally, it has been long observed that on the onset of cancer naturally soft tissues become stiff.

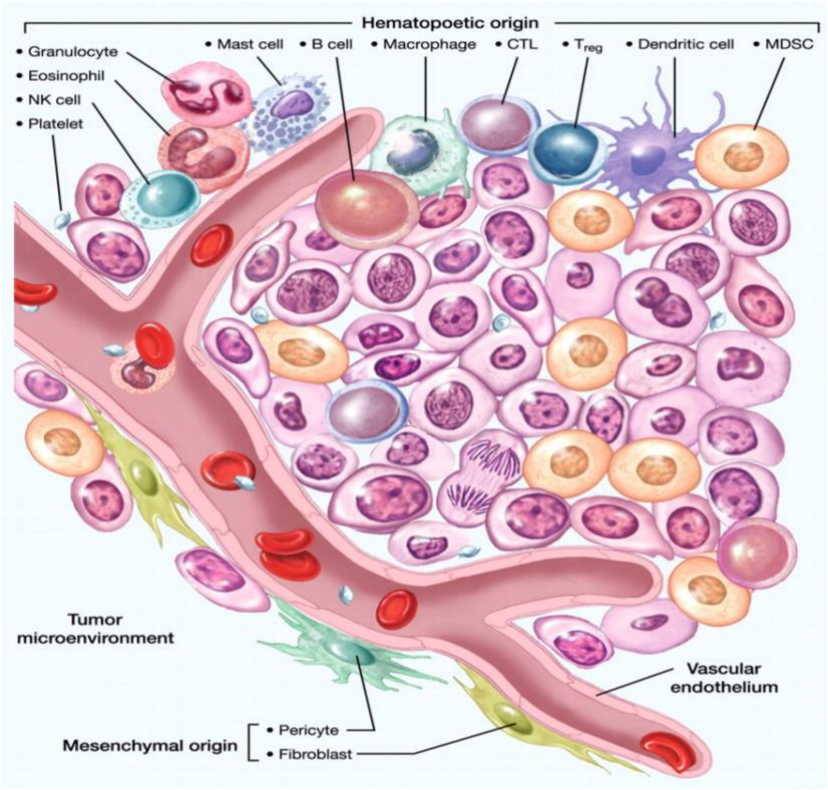

Figure 2.3: Cellular infiltrates within the tumor microenvironment. These cells coordinately form a complex regulatory network that fosters tumor growth by creating an environment that enables cancers to evade immune surveillance and destruction – Cellular Constituents. [Figure taken from [8]].

In epithelial tissue, the ECM stiffness has been reported to be 3-25 times higher than its normal range of 1-38 kPa when malignant (Fig. 2.4A). Moreover, invasiveness and ECM stiffening due to malignant matrix deposition occurs in congruence with the activation of critical mechanosensing signaling pathways involved in promoting metastasis, cancer stem cell-like phenotype, and maintaining CAF identity [73]. These mechanosensing and transduction signaling pathways allow cancer cells to sense and adaptively respond to their physical environment, with soft matrices facilitating epithelial-to-mesenchymal transition (EMT) phenotype and invasive motility, while

stiff matrices triggering cancer stem-cell-like characteristics, increased matrix deposition, and the promotion of metastasis (Fig. 6B) [74].

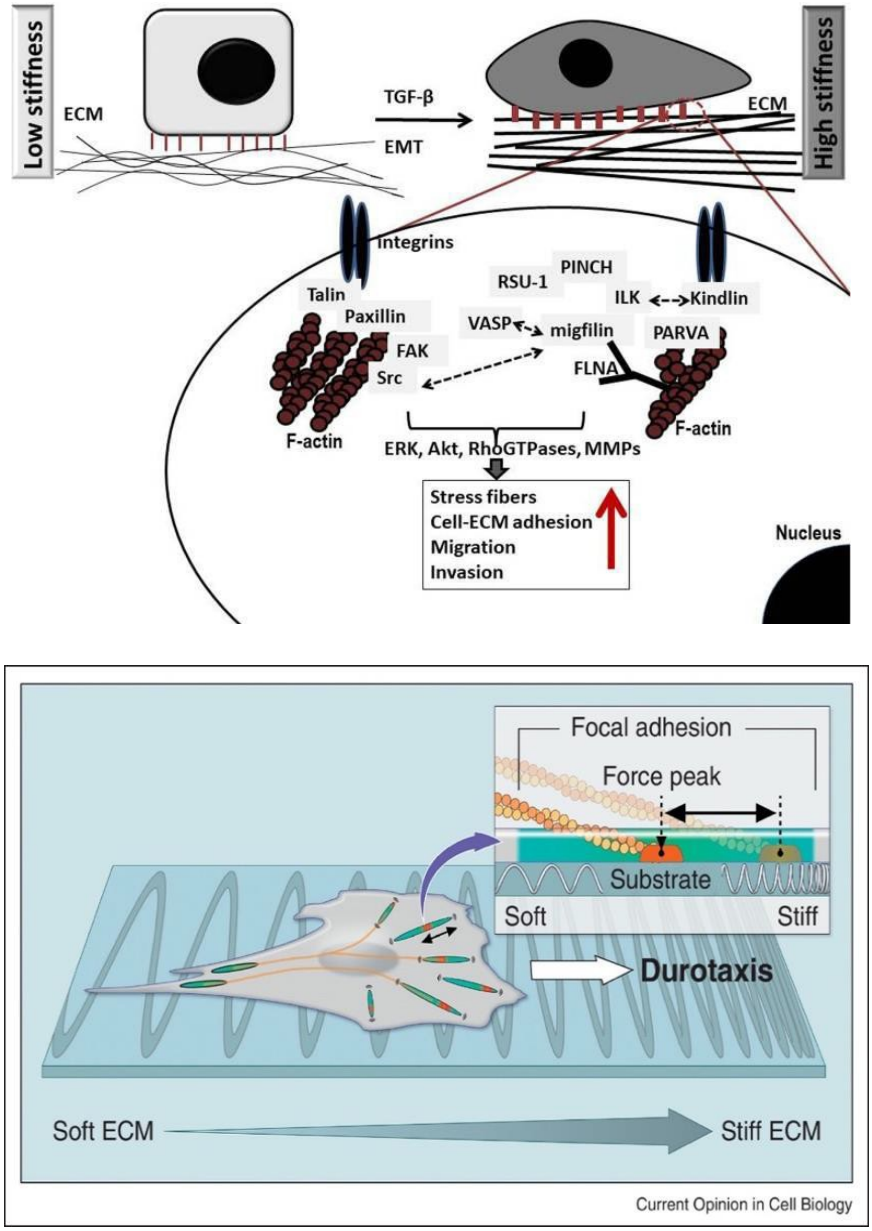

Figure 2.4: (A) Schematic representation of critical protein-protein interactions at cell-extracellular matrix (ECM) adhesion sites in cancer cells grown in low [2-7 kPa] (left) and high [13-18 kPa] (right) stiffness conditions. Several important protein complexes are formed at the cell–ECM sites that are vital for normal cell function. (B) Nanoscale fluctuations of traction forces mediate ECM rigidity sensing and guide directed cell migration. Dynamics of traction forces within individual Fas are essential to direct cells towards stiff ECM. [Figures taken from [9,10].

2.4 Malignant Ovarian Cancer and Metastasis

Cancer cells generally differ from non-cancer cells in their capability to spread throughout the body through two related mechanisms: invasion and metastasis. While invasion involves the direct extension and penetration by cancer cells into neighboring tissues, metastasis is the process by which cancer cells move to another place. Invasion occurs when following proliferation and the progressive increase in tumor size, cancer cells breach barriers between tissues and extend into adjacent tissue. This is known as local invasion, and typically is the first stage in the development of secondary tumors or metastases (Fig. 2.5A).

During the process of metastasis cancer cells penetrate the lymphatic system and blood vessels, and circulate through these systems to finally invade normal tissues elsewhere in the body (Fig 2.5B) [28,75,76]. In both invasion and metastasis, decreased synthesis of substances that bind cancer cells to neighbor cells, together with the abnormal synthesis of enzymes capable of degrading the bonds between cells and tissues, allow the cancer cells to escape the primary tumor site [77,78]. The sequential events that need to be completed for a cancer cell to metastasize successfully, is called the metastatic cascade. The metastatic cascade includes the loss of adhesion between cells, resulting in the dissociation of the cell from the primary tumor, and subsequently the ability of the cell to attain a motile phenotype via changes in the cell to matrix interaction.

The detachment and escape of cells from the primary tumor is orchestrated by a process known as epithelial-to-mesenchymal transition (EMT). This is a dynamic

process wherein epithelial cells go through multiple biochemical and morphological changes enabling them to assume a mesenchymal phenotype with enhanced migratory and invasive capabilities [79–81].

EMT involves a change in cadherin and integrin expressions, and an increase in proteolytic pathways, leading to a mesenchymal morphology and increased invasive potential (Fig. 2.5). EMT is a phenomenon typically associated with epithelial cells in which the normal physiological state is characterized by a lack of vimentin [82–84].

EMT characterization varies slightly between cancer types, however, there are consistent occurrences such as increased expression of mesenchymal marker vimentin, accompanied by decreased epithelium like cytoskeletal morphology and increased elongated mesenchymal-like cytoskeletal morphology. These changes and the induction of proteases for extracellular matrix (ECM) degradation allows for OvCa cells to disseminate from the primary tumor into the peritoneal cavity, where they must then overcome anoikis, before undergoing a mesenchymal to epithelial transition (MET), to seed on the peritoneal wall or omentum and have access to important components of the stroma, such as a rich supply of CAFs [73,85,86].

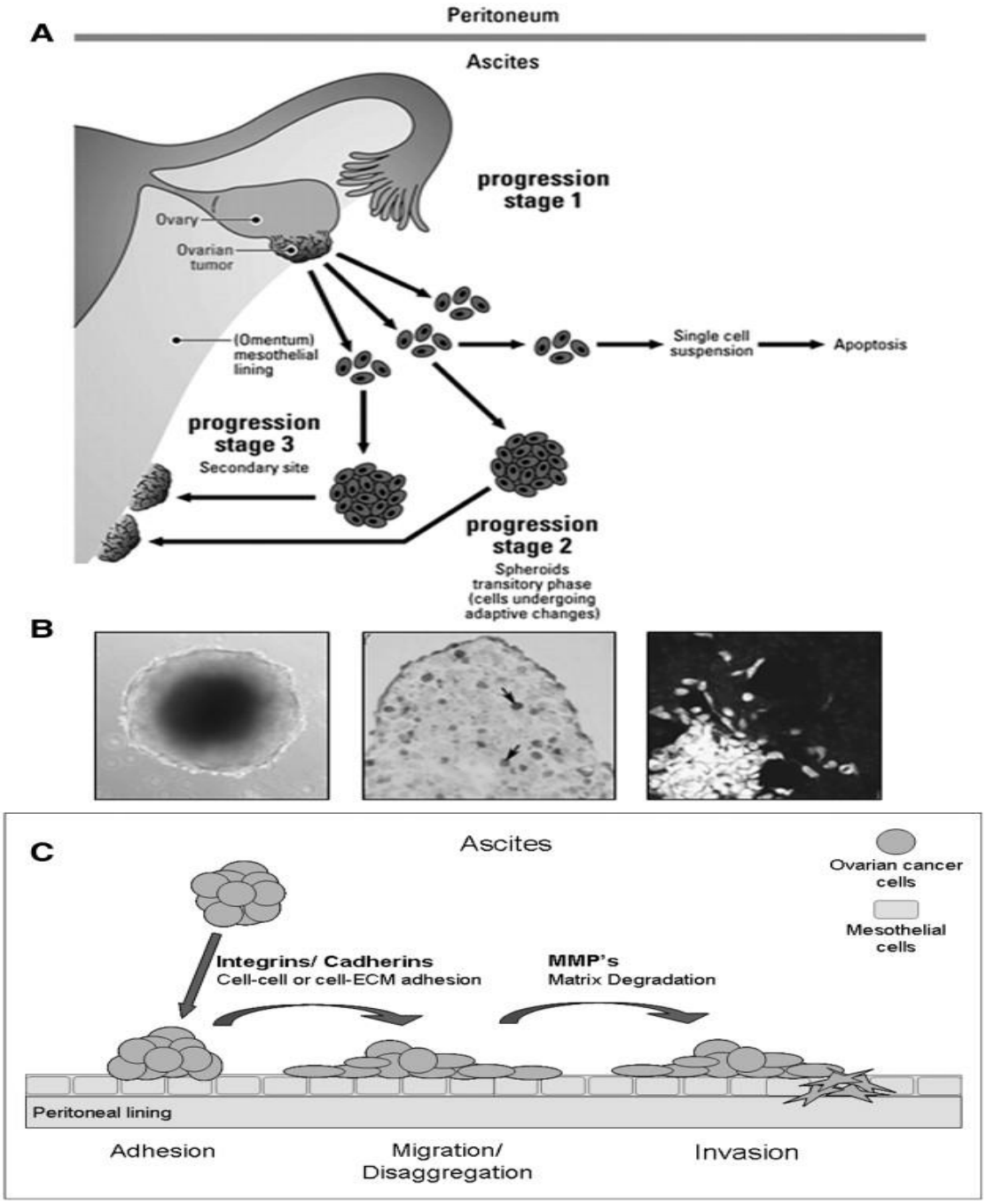

Figure 2.5: Effect of epithelial-to-mesenchymal (EMT) plasticity during ovarian cancer progression. (A) The progression of OvCa spheroids from the peritoneum, to spheroid formation (B), and ascites (C). [Figures taken from [11,12]].

2.5 Treatment Approach of Malignant Ovarian Cancer

The deteriorating prognosis of OvCa patients lies in the fact that 3D spheroid tumor formation can decrease tumor sensitivity to biotherapies. Studies are showing that the current treatment approach with chemotherapeutics may be inducing EMT, thus it is crucial to better characterize biochemical and physical mechanisms behind the disease progression [65,87,88]. There is increasing research suggesting that a multifaceted therapeutic approach is more beneficial. The development of differential subtype and stage-specific treatments have shown potential for improved survival, especially as different cancer subtypes have been shown to exhibit a different response to chemotherapy [89].

Recently, epigenetic therapy has been proposed as a mechanism for upregulating or downregulating oncogenes to sensitize tumors to immune checkpoint therapy [74,90–92]. DNA hypermethylation can result in the emergence of tumor phenotypes [93], and OvCa is known to show Tumor Suppressor Gene (TSG) silencing, via hypoacetylation [22,94,95]. The deacetylation of the DNA promotes the downregulation of many onco suppressing genes, which may be inhibited by histone deacetylase inhibitors (HDACi) (Fig. 2.6). HDACis can up-regulate a wide range of genes involved in immune signaling in breast, lung, colon, and ovarian cancer cells [95,96].

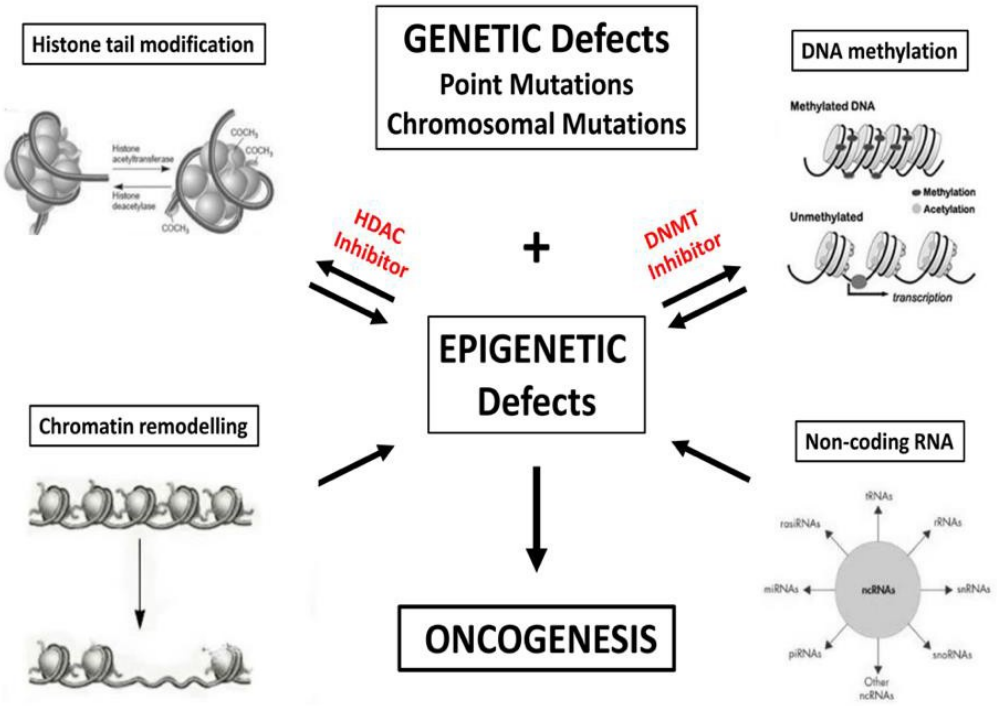

Figure 2.6: Epigenetic treatment mechanism. (A) Oncogenesis is the consequence of genetic as well as epigenetic alterations of the cell. [Figure taken from [13]].

2.6 Effect of SAHA on Ovarian Cancer

Suberoylanilide Hydroxamic (SAHA) (Fig. 2.7) is a novelty drug that was first introduced as a treatment for lymphoma and is currently being evaluated in clinical and pre-clinical studies for its use on OvCa [97]. HDACi is used to provide global OvCa epigenomic disruption, potentially removing TSG silencing [98]. There is considerable evidence suggesting that it affects transcription factors that regulate gene expression of molecules related to aggressive phenotypes, such as those involved in proliferation, apoptosis, cell motility, and angiogenesis [13,95,99]. Moreover, SAHA is known to revert previously chemoresistant cells to a non-resistant phenotype by suppressing proliferation, inducing apoptosis, reducing migration, and reducing invasion due to an

upregulation of caspase-3 and caspase-8 and a downregulation of cyclin B1, ERK1/2, and MMP-9 [96,98,100].

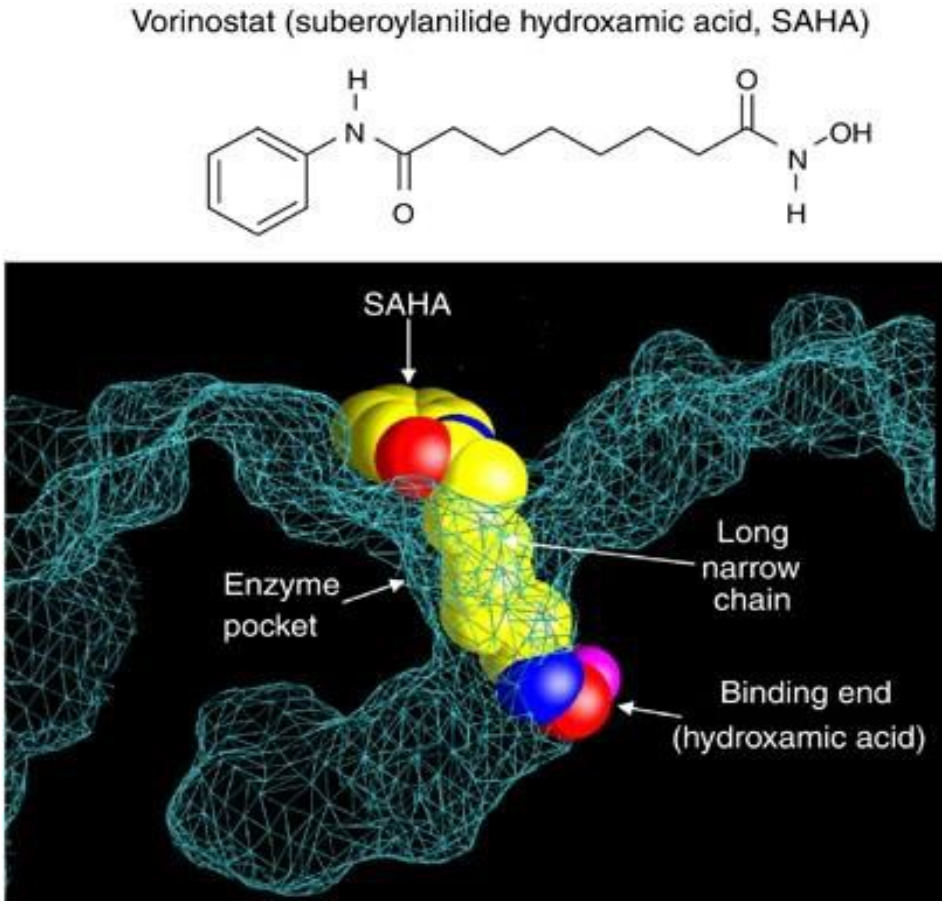

Figure 2.7: Structural features and Schematic representation of the crystal structure of the histone deacetylase like protein with SAHA (vorinostat) that inserts into the zinc molecule at the catalytic pocket. [Figures taken from [14]].

Studies conducted on SKOV3 and OVCAR3 have shown that SAHA inhibits growth while inducing expression of tumor suppressor genes, apoptosis, G2/M arrest, and autophagy [101]. In a study conducted by Liu et al., SKOV3 and OVCAR3 primary cancer cells were isolated from malignant ascites with stage III OvCa and their cytotoxic activities were evaluated by caspase-3 activation before and after SAHA and Paclitaxel treatment [100]. Concentrations of 1-20 μM of SAHA were found to kill chemo-

resistant cells and be as efficient in inducing cell death as Paclitaxel at concentrations of 3-300 nM. SAHA seemed to act selectively on gene expression, induced growth arrest, and induced apoptosis at similar levels to Paclitaxel.

As also shown by Chen et al., cells that were exposed to SAHA treatment, showed higher levels of acetyl-Histone H3 and H4 expression levels when compared against the aggressive behaviors of ovarian carcinoma, indicating a potential increase in chemo-sensitivity [99]. Moreover, other studies showed a reduction from 67% to 48% in OvCa cells when treated with combined Paclitaxel+SAHA treatment as opposed to just paclitaxel. The combined treatment also reduced migration by the induction of cell-cycle arrest, apoptosis, and autophagy through upregulation of tumor suppressor genes p16 and p53 and inhibiting PI3K/AKT/PTEN signaling pathway. Interestingly, as seen by several studies such as the one by Mrakovcic and co-workers, HDACi activity seems to be selective towards cancerous cells and is ineffective at killing normal cells under cancer-treating concentrations [98]. These observations indicate the possible synergistic antitumor effects of SAHA treatment [41,102,103].

CHAPTER 3 METHODS AND MATERIALS

3.1 Micropatterned Substrate Fabrication

Si-TiB_2 substrates were fabricated at the University of Houston, Department of Electrical and Computer Engineering, using varying techniques in the fabrication of integrated circuits. Silicon nitride was deposited on top of a silicon wafer base, followed by thermal oxidation to form silicon dioxide. Molten titanium diboride was then deposited evenly over the silicon wafer before prefabricated chromium masks were used as a negative photoresist to pattern circular designs of TiB_2 of varying diameters. The material was wet-etched from non-patterned areas using 30% hydrogen peroxide, leaving behind TiB_2 patterns. Substrates were then cleaned in deionized water, acetone, and isopropyl alcohol. They were then transferred to ethanol and later dried using a compressed nitrogen (N_2) air gun. The experimental evaluation included the following substrate types, silicon (Si) only, titanium diboride (TiB_2) only, and silicon background with micropatterns of titanium diboride (Si-TiB_2). Patterns consisted of variably sized circles, ranging from diameters of 200μm to 500μm.

3.2 Si-TiB_2 Substrate Surface Characterization

Atomic force microscopy (AFM) was performed at the AFM-SEM core of the Houston Methodist Hospital Research Institute. The surface topography and the root-mean-square roughness (Rrms) of the substrates were examined by atomic force microscopy. Peak Force Quantitative Nano Mechanics was performed in the air to ascertain measurements as per manufacturer instructions. The deflection error sensitivity was calculated to be 62.97 nm/V. Images were processed and analyzed with

Bruker NanoScope Analysis software version 1.40 to measure surface roughness (Rq) [104,105]. Three separate areas (of 25 μm2 each) were collected for each surface type and Rq was calculated on subareas of 500x500nm, with a total of about 60 Rq values for each surface type.

3.3 Cutting and Cleaning Substrate

Substrates were manually cut into small squares or rectangles, generally between 10-20 mm2 in area, using a diamond-tipped pen. Before seeding, substrates placed in clean glass petri dishes with enough deionized water to cover the substrate, and the glass petri dish was placed in a deionized water-filled ultrasonicator were for 2-3 minutes. They were then individually scrubbed with a cotton-tipped applicator, followed by the removal of liquid using an aspirator. This process was repeated in acetone, isopropyl alcohol, and deionized water. After this, substrates were transferred to a 70% ethanol solution, imaged and measured, then dried with an air gun in a sterile biosafety cabinet. Once dry, they were ready to be seeded with cells.

3.4 OVCAR3 and SKOV3 Cell Line Passaging & Seeding

At around 75-85% cell confluency, SKOV3 and OVCAR3 cell lines were regularly passaged to new flasks. Cells were washed twice in 3 mL 1X phosphate-buffered saline (PBS) (Sigma-Aldrich H6648). PBS was aspirated, and cells were incubated with 3 mL of 0.05% 1 mM Trypsin from bovine pancreas (Sigma-Aldrich 59417) in a 37°C humidified, 5% CO_2 incubator until cells had detached (3-5 min). The detachment of cells was visualized under a phase-contrast microscope. When cell detachment had taken place, 3 mL of Cancer Media (CM) (20% RPMI 1640 with

glutamine (02-0205 VWR Life Science), 1% antibiotics (Sigma-Aldrich A5955), and 0.1% insulin (ABM TM053)) was added to the flask. This was followed by transferring the 6 mL solution from the flask into a 15 mL tube for centrifugation. Solutions were centrifuged at 98 rcf for 4 minutes in order to form a cell pellet. The supernatant was aspirated, and 1 mL of fresh media was added to resuspend the pellet in solution and achieve a uniform suspension of the cells. After which, 12 µL of cell suspension was added to a hemocytometer, and cells were counted to establish a cell concentration. Cells were then added to a new culture flask, normally at an amount of 250,000 cells in 5 mL CM. This number was increased or decreased, depending on when confluency for seeding was required.

Substrates would be seeded at the same time as passaging, and thus would follow the same initial protocol. After cells were counted, the suspension would be diluted or concentrated to a final concentration of 1200 cells/µL. Substrates that had been imaged and area measured would be placed at the edge of 24-well plates and then seeded individually based on their surface area (volume = ½ area of the substrate), to achieve the desired seeding density (600 cells per mm2). Substrates were left for 5 minutes to allow cells to settle, then 1 mL of culture media (CM supplemented with 10 ng/mL human FGF2 (Sigma-Aldrich F0291) + 1% heparin (Sigma-Aldrich H3393) would then be gradually added to each well, in such a way as to minimize any disturbance to the cell droplet placed on the substrate. Substrates were then carefully transferred to a humidified incubator at 37°C with 5% CO_2.

3.5 Stereomicroscopy

After cleaning, substrates were imaged with an Olympus S2X7 Microscope at 1x resolution. This image was used to calculate the surface area of the chip, to determine the volume of cell suspension required for seeding at the desired cell density. The free-form select tool was used to select the edges of imaged substrates and calculate the enclosed surface area. Each substrate was imaged prior to seeding by acquiring images in quadrants to create a set of template mask images, to be used as the background reference images for longitudinal monitoring of cell growth. Generally, one-four separate template images were taken, to capture the entire surface of the substrates. This was subject to substrate size, with fewer images for smaller ones. During experimentation, images were taken along similar quadrants as defined by the template mask images, at 2.5x magnification to visualize cellular growth on the substrates as well as for documenting aggregate formation. These images were taken before seeding, on day one after seeding, and then every 24-48 hours to monitor cell growth. Substrates were imaged by carefully removing them from their respective wells, before transferring to a 35 mm petri dish containing supplemented CM.

3.6 Epigenetic Drug Treatment

A stock solution of SAHA (Cayman Chemical Company, #10009929) was made to 5 mM, in DMSO (Sigma-Aldrich D8418). SAHA was diluted into CM supplemented with FGF2 and heparin. SAHA was introduced onto the substrates where aggregates had already been formed (at day seven after seeding). The concentrations used were 1

μM, 3 μM, and 5 μM [106], finally deciding on a sub-lethal dosage of 3 μM for all our reported data.

3.7 Antibody Staining Protocol

Cells were grown on substrates until the desired time point of growth was reached. Immunofluorescence imaging was then used to assess functional phenotype with cell-specific monoclonal antibodies. Cells were fixed in 4% paraformaldehyde (Electron Microscopy Science 15710) /1X PBS for 15 minutes. They were then washed twice in 1X PBS for 5 minutes, before blocking in 5% donkey serum/0.15% Triton-X 100 (Jackson ImmunoResearch Laboratories 017-000-121) / 1X PBS for 1 hour, then washed again twice with 0.2% Triton-X 100/ 1X PBS. Cells were then stained with primary antibodies by inverting the substrates face down in 80 μL of antibody solution placed on parafilm lined petri dishes, and then being left covered with foil overnight in a fridge at 4°C. Primary antibodies included: Vimentin (1:200, rabbit monoclonal anti-vimentin, Abcam ab16700), and Ki-67 (1:100, mouse monoclonal anti-Ki67, Santa-Cruz Biotechnology, sc-2390).

Following incubation in primary antibodies, substrates were washed with 1X PBS twice and then incubated in secondary antibodies, by dropping them face down into 80 μL of solution placed on parafilm lined petri dishes and left for an hour at room temperature in the dark. Secondary antibodies were purchased from Jackson ImmunoResearch Laboratories and included, Phalloidin-iFluor 488 reagent ab176753 (1:1000) and Alexa-Fluor 594-AffiniPure Donkey Anti-Rabbit (1:500). After the second incubation and two washes in 0.2% Triton-X 100/ 1X PBS, 10 μL of 0.02 mg/mL

DAPI (Biotium, 40043) was added to the solution, and cells were allowed to stain for 15 minutes in the dark. Substrates were transferred to glass slides, and a droplet (~24 μL) of VECTASHIELD Antifade Mounting Medium (H-1700 Vector Laboratories) was dropped on top of each, prior to imaging.

Stained substrates were imaged using the Olympus Fluoview 1000 Confocal Microscope and imaged at 4x and 20x magnifications. Three to five images of circle varying in size patterns (200, 250, 300, 350, 400, 450, 500μm) per substrate at each time point and magnification were saved (DAPI excitation: 405 nm, F-actin excitation 488nm, Vimentin excitation: 533nm, and Ki-67 excitation 633nm).

Alternatively, viability staining was carried out by transferring substrates to 1.5 mL of 1X PBS in a 35 mL petri dish. In the dark, 0.5 μL of 10 mg/mL Acridine Orange (AO, Biotium, 40039), 0.5 μL of 1 mg/mL Propidium Iodide (PI, Biotium, 40017), and DAPI at a concentration of 5 μM was added. AO stains the DNA of live cells, and PI is a membrane-impermeable dye that only enters dead cells with damaged plasma membranes. Samples were left in the dark for 20 minutes, before confocal microscopy (DAPI excitation: 405 nm, AO excitation: 488 nm, PI excitation: 533 nm). Analysis of stained cells was carried out with the Fiji/ImageJ [107], utilizing custom-written scripts to determine the percentage of viable cells covering the circular TiB_2 patterns.

3.8 Statistical Analysis

A macro designed for ImageJ was created and used to determine the percentage of viable cells growing on the TiB_2 micropatterns at different days following seeding. At least three to five images of circle varying in size patterns (200, 250, 300, 350, 400,

450, 500μm) from each substrate at each time point were analyzed. The macro automatically computed the thickness of aggregates from z-sections of images of the DAPI stained nuclei, while manual delineation of the aggregate boundary was used to compute the diameter of the aggregates. The computed viability was reported by giving a percentage of AO versus PI stained cells in a given aggregate.

Statistical analyses were carried out with PHStat in Excel. Comparison of statistical differences between multiple data sets (> 2) was carried out with ANOVA and a Tukey-Kramer test, while comparisons between two data sets were carried out with a Student's T-Test. Significance was regarded as $p < 0.05$. Viability confidence interval estimate for the mean was obtained by pooling together one repeat of experiments from days 7 and 9 that had similar viability using ANOVA test for comparisons. Statistical comparison of the architecture (diameter and thickness) of aggregates on different diameter circles were done by ANOVA test, by pooling together data of aggregates on the same size patterns of the micropatterned substrates from different repeats.

CHAPTER 4 RESULTS

4.1 Surface Characterization of Micropatterned Substrates

Stereomicroscopy images of Si, nonpatterned Si-TiB_2, and Si– TiB_2 with circle patterns with diameters ranging from 200 to 500 μm (Fig. 4.1). Si areas appear darker compared to TiB_2 which is relatively brighter.

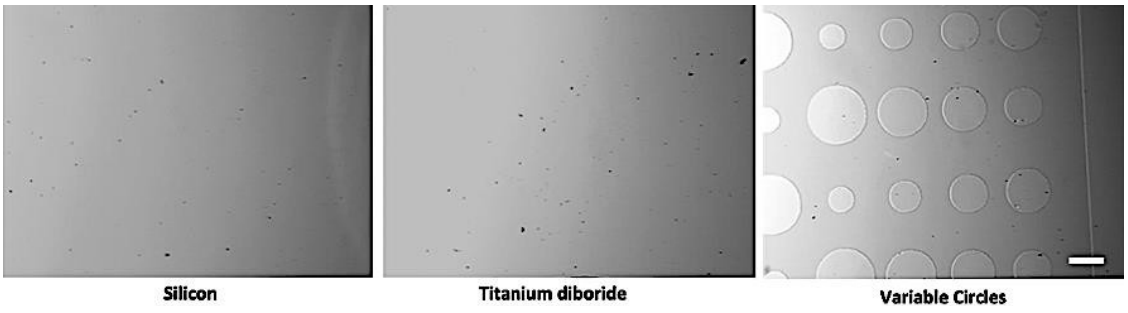

Figure 4.1: Stereomicroscope images of substrates taken at a magnification of 2.5x. Substrates of Si, unpatterned TiB_2, and Si-TiB_2 with micropatterns of circles of varying diameters are shown. (scale bar 200 μm).

The novel combination of Si and TiB_2, differing in material stiffness, hardness, roughness, wettability, and surface charges, is amenable to microfabrication processes and supports extended cell culture. In previous work, we have shown that the Si-TiB_2 substrates promote preferential and selective cell growth behavior via substrate mediated protein adsorption [56]. Importantly, growth factors with a heparin-binding domain in conjunction with heparin play a dominant role in establishing specific cell growth on the TiB_2 micropatterns. In their absence, cells exhibit preferential attachment to TiB_2 patterns versus Si (i.e., more cells attach to micropatterns versus the Si background), whereas highly selective growth (i.e., cells attaching only to

micropatterns) is observed in media supplemented with heparin and growth factors that have a heparin-binding domain.

Critically, protein-mediated micropattern specificity is not limited to a particular growth factor supplement or combination; rather, any individual growth factor with a heparin-binding domain can be used to achieve TiB_2 pattern-specific growth and 3D aggregation. In this study, we utilize supplements of basic fibroblast growth factor (FGF2) with heparin to achieve micropattern specific ovarian cancer cell growth. FGF2 plays a key role in chemotaxis and focal adhesion formation. According to previous research, FGF2 is known to have an impact on cellular adhesive properties and cell-cell communication [108]. Based on our previous work [56], it was determined that there was no significant difference in protein adsorption on chips between 10, 50, and 500 ng/mL of FGF2. For this reason, we chose to supplement our culture media with FGF2 at a dosage of 10 ng/mL. Thus, to utilize the adhesive proteins adsorbed from the supplemented media and optimize the conditions for cellular growth, we chose to use cancer media supplemented with FGF2 and heparin.

Furthermore, heparin is known to induce FGF2 stimulation, which is responsible for cell growth and proliferation [109]. Heparin and FGF2 [110] can also induce chemotaxis and may also play a role in the adhesive properties of cells to TiB_2 micropatterns via the formation of focal adhesions [10,111]. To observe differential protein deposition, Atomic Force Microscopy (AFM) was carried out on clean substrates which had been incubated overnight in cancer media supplemented with 10 ng/ml FGF2 and 1% heparin [106] (Fig. 4.2).

AFM is a surface probe method of line-scanning the surface to detect nanoscale topographical changes [109,112]. All substrates were scanned, to detect alterations in surface topography and roughness, aligned with protein deposition. Nonpatterned Si-TiB_2 substrate incubated in cancer media (CM) supplemented with 1% heparin and 10 ng/ml FGF2, showed a reduction in the layer of protein deposition over the substrate as opposed to the one supplemented with FGF2 only. On the other hand, Si only substrates incubated in cancer media with 1% heparin and 10 ng/ml FGF2 showed a visibly greater reduction in protein deposition (Fig. 4.2). This demonstrates that heparin causes a differential protein deposition on Si versus that on TiB_2. Moreover, the topography of protein deposition on the TiB_2 area is qualitatively relatively uniform while the Si area shows random clumping of protein deposits.

Overall, AFM results suggest that the addition of heparin causes a visible loss of deposition for proteins to Si, but not TiB_2. These results suggest that heparin has some form of binding interaction with growth factor proteins, which aligns with heparin's known induction of FGF2 receptor binding, as well as having an affinity for other growth factors, such as VEGF [104,113].

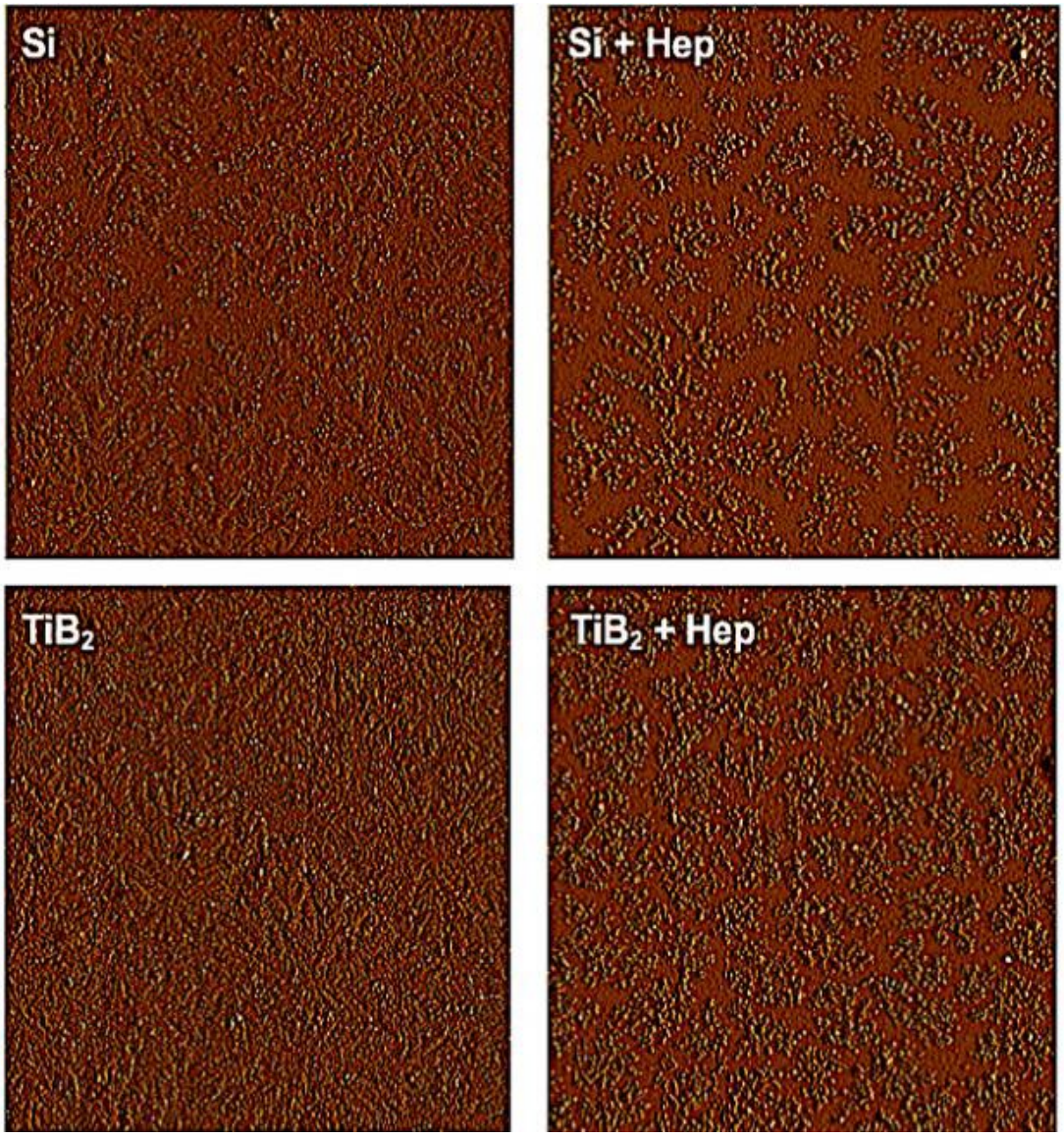

Figure 4.2: Surface characterization of micropatterned substrates. A panel of four substrates (clockwise): Silicon (Si) with FGF2 without heparin, nonpatterned Si-TiB_2 with FGF2 without heparin, nonpatterned Si-TiB_2 with 1% heparin and FGF2, and Si with 1% heparin and FGF2. High-resolution topography images showing Si area with visibly reduced protein deposition caused by heparin addition compared to TiB_2.

Increased surface roughness has also been shown to result in increased cellular adhesion, proliferation, and lower cytotoxicity [105]. In a previous study, we determined the average roughness (Rq) for Si was 0.16 nm, whereas the average Rq for TiB_2 was 0.28 nm. These roughness values are both in the same category of surface

finishes; N1 of the German-Swiss norm series [114]. However, a study conducted by Mutreja et al. indicated that the roughness of Ti increased adhesion and proliferation of cells [115], and a study by Shiozawa et al. indicated that slight differences in Ti and Ti alloys' roughness impacted cell adhesion and allowed for directional cell growth in nanopatterns [56]. This shows that TiB_2 has an impact on cellular proliferation and aggregation, despite only being slightly rougher than Si.

4.2 Growth of SKOV3 and OVCAR3 on the Micropatterned Substrates

Previous studies have shown that culturing cells on our novel Si-TiB_2 micropatterned substrates promotes cellular patterning and the formation of 3D aggregates in mesenchymal stem cells [106]and ovarian cancer cells [116]. In this study, we assessed our micropatterned substrate for its potential to support a 3D microenvironment for two ovarian cancer (OvCa) cell lines, SKOV3 and OVCAR3.

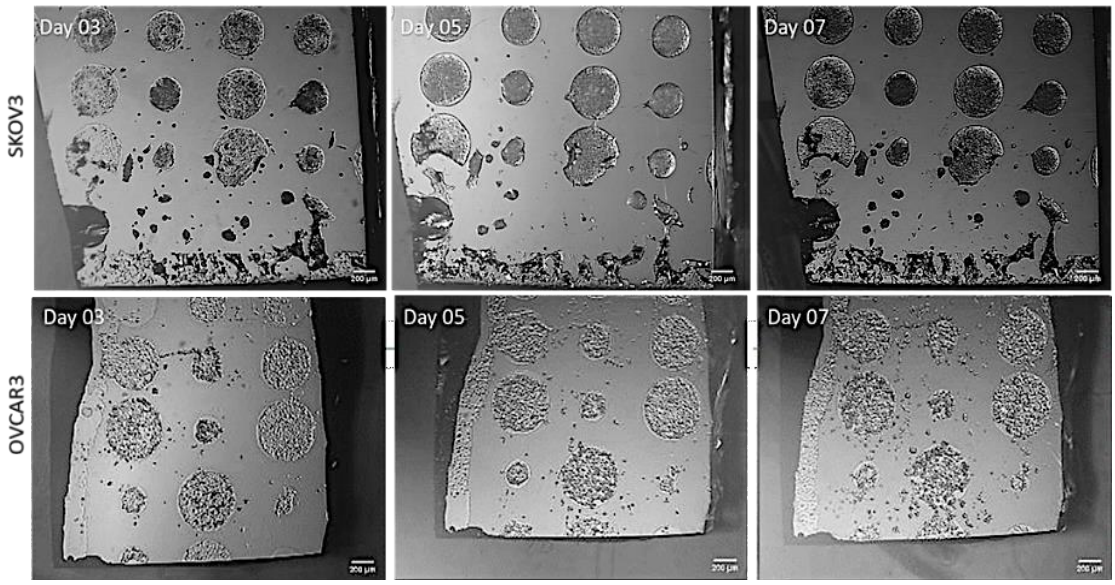

Figure 4.3: SKOV3 and OVCAR3 growth on the Si-TiB_2 micropatterned substrates. Representative reflected light images from the stereomicroscope images of SKOV3 at 24-48 h are shown in the top row, and the bottom row shows images of OVCAR3 over a week in culture (scale 200 μm).

We evaluated the ability of OVCAR3 and SKOV3 to adhere and grow on the Si-TiB_2 micropatterned substrate over a one-week period through acquiring stereomicroscope images at intervals of 48h. Representative reflected light images from stereomicroscopy of OVCAR3 and SKOV3 cultured on the Si-TiB_2 substrate over a week are presented in Fig. 4.3.

Following a week in culture, both OVCAR3 and SKOV3 maintained specific growth on the TiB_2 circle micropatterns, with SKOV3 spontaneously forming cellular aggregates and OVCAR3 maintaining monolayer growth. This is similar to the findings of Heredia-Soto et al., who used ultra-low attachment plates and noticed that OVCAR3 formed either monolayers or loose aggregates, while SKOV3 and other cell lines with mesenchymal morphology seemed to form more compact and well-defined spheroidal aggregates [117].

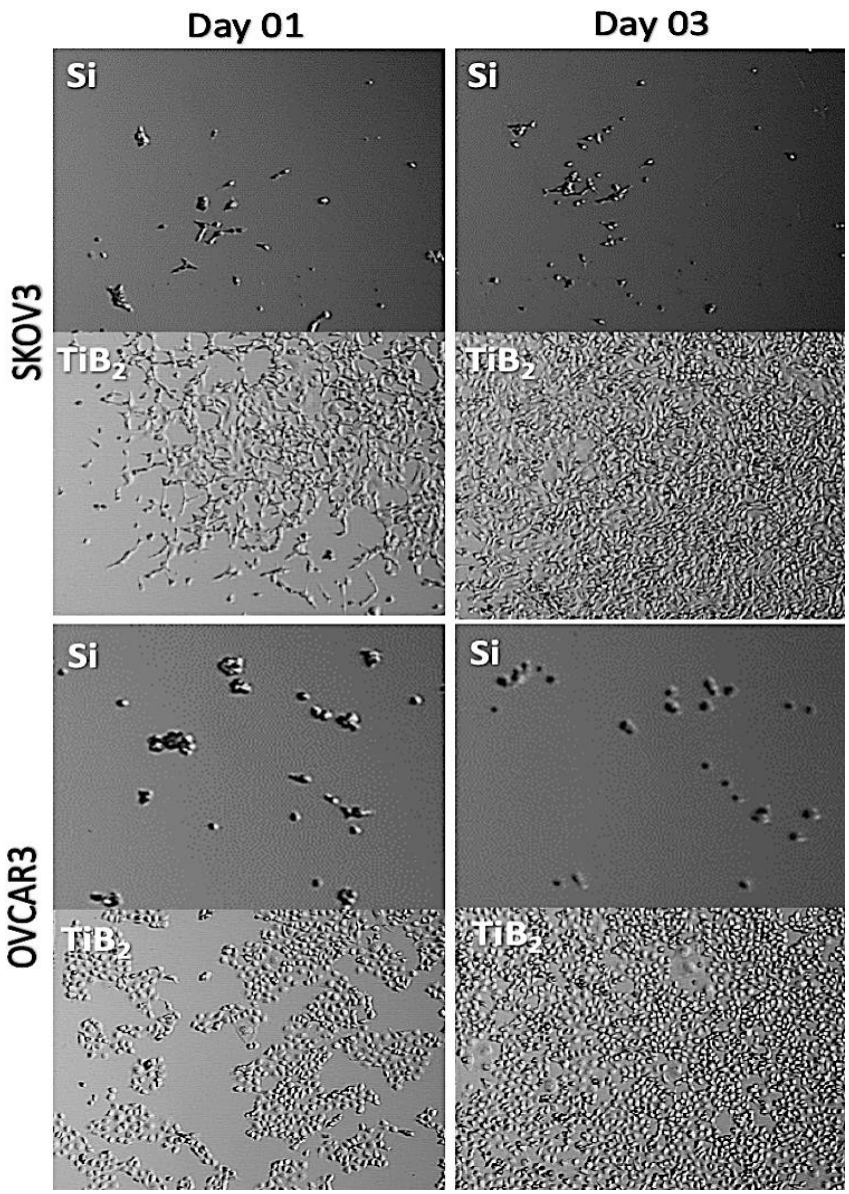

Figure 4.4: SKOV3 and OVCAR3 growth on the Si and TiB_2 substrates. Representative reflected light images from stereomicroscopy at days 1 and 3 are shown.

Interestingly, assessment of cell growth on the Si only substrate over a three-day period revealed that both OVCAR3 and SKOV3 struggle to maintain adherence. OvCa cells from both cell lines eventually detached from the substrate altogether (Fig. 4.4). On the other hand, cell growth on the TiB_2 only substrate showed both cell lines proliferated and adhered well. Thus, we can see a stark preference for the TiB_2 surface.

4.2.1 Intercellular Bridges

Direct intercellular communications are an important feature for tissue homeostasis. However, the formation of these channels is even more important to cancer cells [118,119]. In cancer cells, intercellular interactions have been described as gap-junctions, intercellular bridges, tunnels, and connexins [120]. Regardless of the name, they all seem to function similarly. A study conducted by Asencio-Barria et al. showed how these intercellular communication channels had been used by cancerous aggregates in 3D cultures to communicate and increase resistance to hypoxia via oxygen and nutrient exchange [121–123].

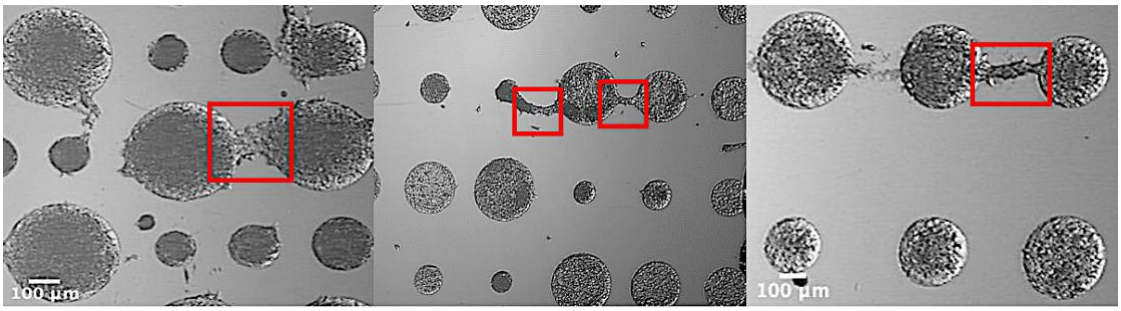

Figure 4.5: SKOV3 growth on the Si-TiB_2 micropatterned substrate. Representative reflected light images from stereomicroscopy. Images wherein intercellular channels are seen forming between SKOV3 aggregates.

Despite their initial inability to grow on the Si background, SKOV3 cells were observed to exhibit the sporadic formation of bridges between cellular aggregates regardless of circular pattern size or spacing between the circle patterns (red boxes; Fig. 4.5). It is plausible that they may represent intercellular communication channels [124]such as those seen in OvCa epithelial cells and spheroids by Lou et al. when imaging replated cells derived from a malignant effusion of a patient with OVCAR3 and cells that were cultured in a clonogenic dilution assay under non-adherent

conditions, under a stereomicroscope, to note direct intercellular communication [48,58,116,125].

4.2.2 Long-Term Culture

Results indicate that TiB_2 micropatterned substrates can result in specific growth. SKOV3 cells successfully attached and grew on TiB_2 micropatterns, generally retaining a high degree of specificity, whereas loss of OVCAR3 specific growth was observed at an earlier time (Fig. 4.6). Cells were grown on TiB_2 substrates for 14 days to observe if the growth remained specific. Both OVCAR3 and SKOV3 lost specificity after day 9, then spread past the circular patterns. More long-term repeats are needed in order to validate results and identify the exact point the loss of specificity occurs.

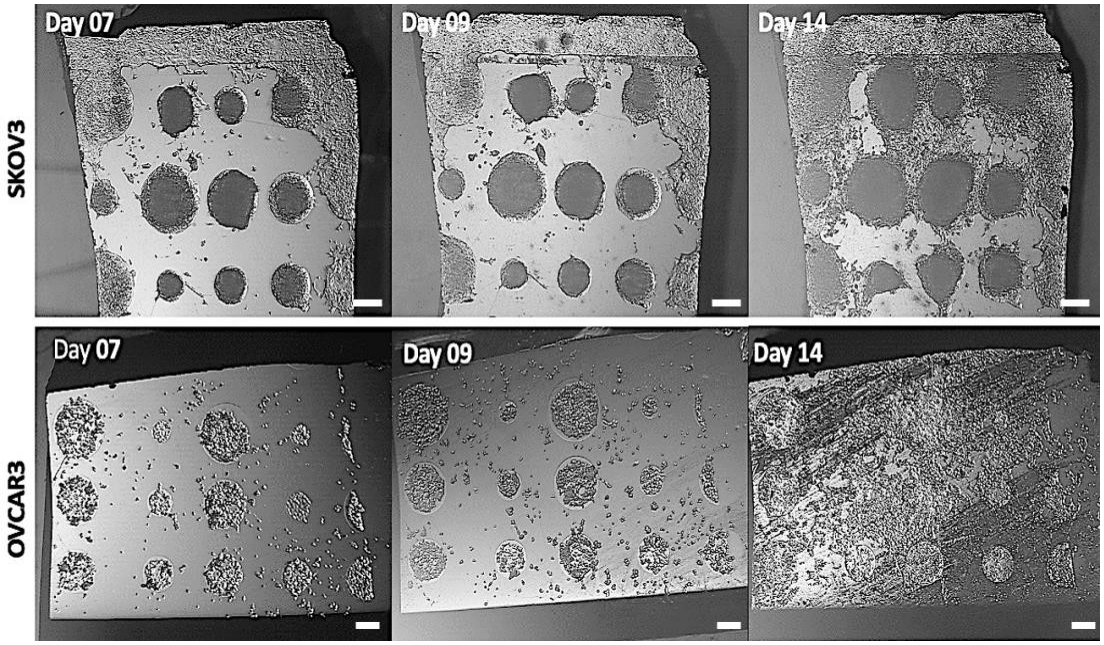

Figure 4.6: Long term SKOV3 and OVCAR3 growth on the Si-TiB_2 micropatterned substrate. Representative reflected light images from stereomicroscopy. Images wherein Si growth past the TiB_2 circles. SKOV3 and OVCAR3. Days 7-14. (scale is 200 µm).

4.3 SKOV3 3D Aggregate Characterization

4.3.1 Size and Viability

Statistical analysis was performed for thickness, diameter, and viability using seven experiments with at least one data point for 200, 250, 300, 350, 400, 450, and 500 μm per experiment. The size of the SKOV3 3D aggregates, in relation to the micropatterns, was evaluated from confocal stacks of DAPI stained nuclei. As reported in Fig. 16, the diameter of the aggregates is dependent on the pattern diameter, with the larger aggregates forming on the larger patterns (n=7, p=0.0000). When evaluating the thickness of the aggregates, it remained uniform ranging from 46 to 54μm in size (p = 0.2881), which is supported by previous 3D culture studies, using ultra-low attachment (ULA) plates and Matrigel, reporting spheroids 30–100 μm [66].

The viability of the SKOV3 3D aggregates is presented in Fig. 4.7C through a maximum intensity projection of AO/PI stained aggregates. Despite the difference in the size of the 3D aggregates produced by the circular patterns, the viability between them ranged from 81-86% with a mean value of 83%, which was as expected based on other studies such as the one conducted by Raghavan et al. reporting 3D spheroid viability at approximately 85% when using novel ULA plates. Their study produced stable and uniform aggregates using a novel well plate system that utilizes a hanging drop array. Each well of the hanging drop array plate contained 30 replicates of 10, 20, 50, and 100-cell spheroids. Their viability was around 85% and didn't decrease dramatically even when treated with cisplatin [83,126–128].

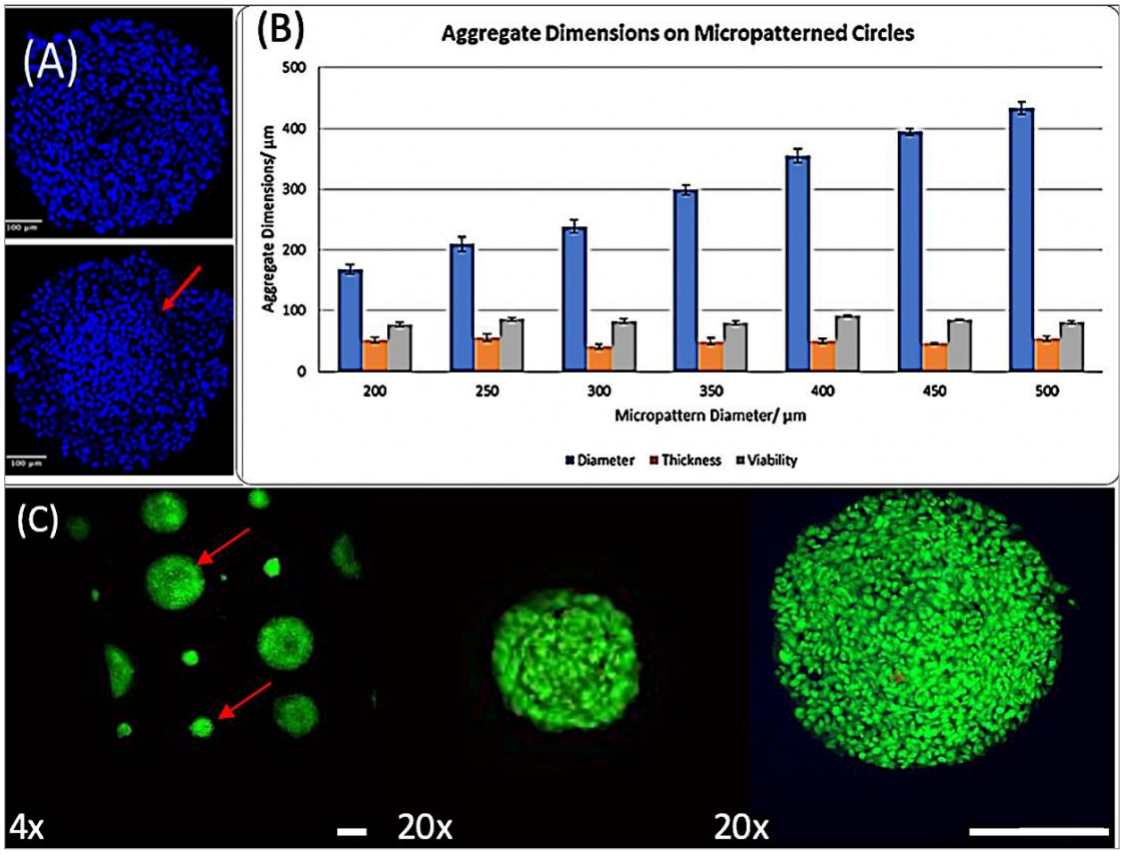

Figure 4.7: Viability and size assessment in SKOV3 3D aggregates. (A) An XY projection generated from confocal z-stacks of the DAPI stained nuclei of a SKOV3 aggregate on a TiB_2 circular micropattern (scale 200 µm). The first panel shows the depth at the bottom of the aggregate and the second panel shows the center of the aggregate with the spheroid in the middle (red arrow) [70µm thickness] (B) a plot of aggregate size (thickness and diameter) against the pattern size (diameter of circle patterns). (C) Maximum intensity projection images generated from confocal z-stacks of SKOV3 3D aggregate on 200 µm and 500 µm diameter circle pattern stained for viability with Acridine Orange (green, live) and Propidium Iodide (red, dead) at 4x and 20x magnifications (red arrows indicate the two chosen aggregates from 4x to 20x) (scale 200 µm).

4.3.2 Phenotype and Morphology

Immunofluorescence imaging was used to assess cytoskeletal morphology and functional phenotype via biomarker specific antibodies. Vimentin is an intermediate filament that is primarily expressed in mesenchymal cells. Its expression in epithelial cells is reported to be associated with the malignant phenotype of cancer cells in vitro,

and thus, it is often used as a marker for cells undergoing an epithelial-to-mesenchymal transition (EMT) [84]. Based on previous studies such as those conducted by Suster et al. [129,130], who used Vimentin to determine "cancer stem cells (CSC)," we chose Vimentin for the assessment of traditional stem cell-like phenotype on SKOV3 (Fig. 4.8) [131,132].

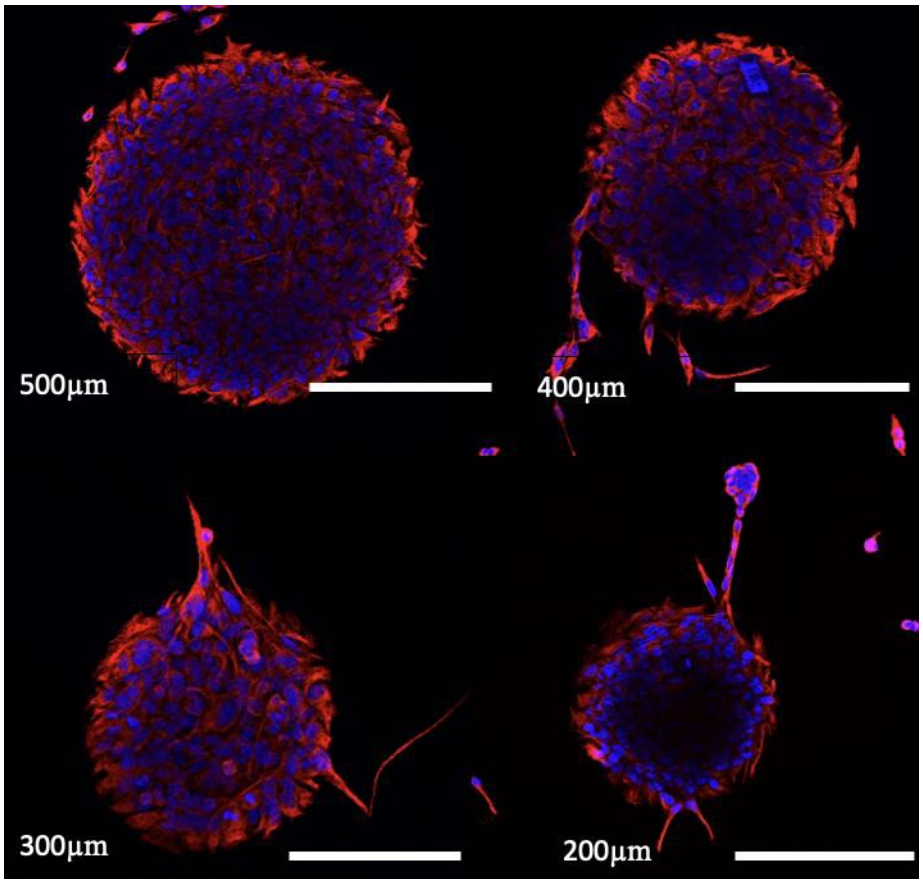

Figure 4.8: Maximum intensity projection images generated from confocal z-stacks of SKOV3 3D aggregate on 200-500 µm diameter circle patterns stained for mesenchymal phenotype with Vimentin (red) and DAPI (blue) at 20x magnifications (scale 200 µm).

Vimentin levels were present uniformly throughout the aggregates over the week-long culturing period, with high levels being concentrated at the interphase of the TiB_2 pattern and Si background (Fig. 4.8). Suggesting the TiB_2-Si substrate does not

have a significant impact on the expression levels of vimentin, which is traditionally reported to be expressed in SKOV3.

F-Actin is a crucial part of a cell's cytoskeleton, which is essential for cell stability, cellular function, and motility [133,134]. It is often seen as an accessible means for visualizing mammalian cell structure via fluorescence microscopy. Studies conducted by Chauhan et al., which have been corroborated by Jalal et al., indicate that F-actin is an ideal biomarker that captures SKOV3's spindle-like morphology [57,135]. Thus, we chose F-actin to capture the structural morphology of the cytoskeleton within SKOV3 aggregates (Fig. 4.9).

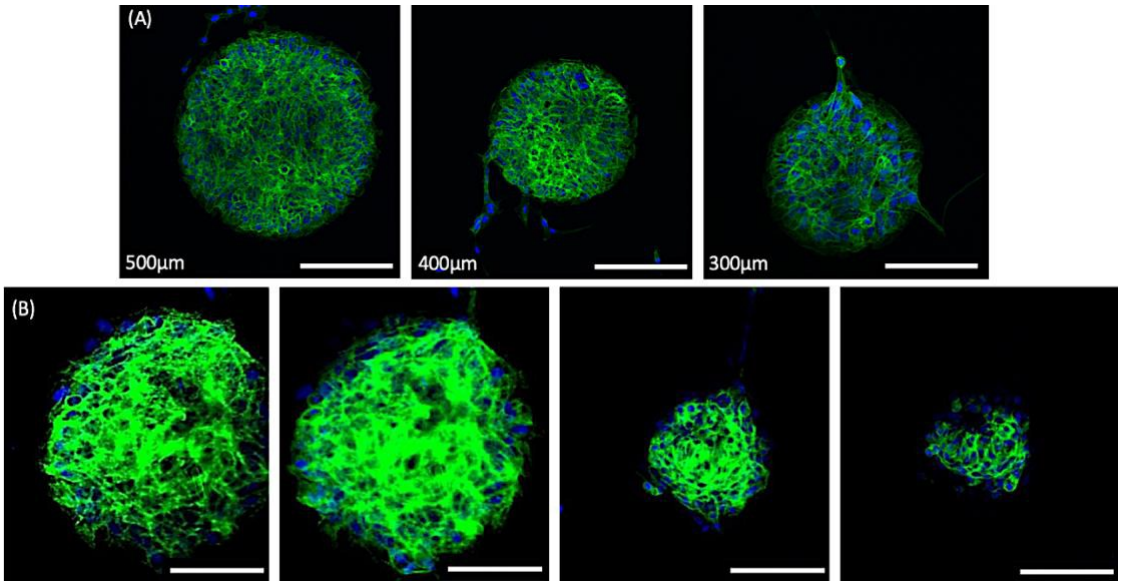

Figure 4.9: Maximum intensity projection images generated from confocal z-stacks of SKOV3 3D aggregates (A) on 300-500 µm diameter circle patterns (B) on 200 µm diameter circle pattern from the center of the aggregate to the bottom. Stained for the cytoskeletal morphology with F-actin (green) and DAPI (blue) at 20x magnifications (scale 200 µm).

The traditionally spindle-shaped stretching associated with monolayer culturing SKOV3 is shown [136–138]. Moreover, the cells within the aggregate (i.e., at the center) are visibly more rounded in shape. The second panel in Fig. 4.9 shows

the variation in cytoskeletal morphology as you migrate through different depths; as you migrate to the higher slice of the aggregate, the cytoskeleton arrangement becomes predominantly rounded.

4.3.3 Proliferation

Ki-67 has been used as a proliferation and tumor growth biomarker for both 2D and 3D tissue culture models in several studies [139–142]. Its expression is strongly associated with tumor cell proliferation, and it is also widely used in routine clinical pathological investigations, prognostics, and assessment of biopsies [143].

Most 3D culture studies on the effect of different drug treatments, such as the Celecoxib experiment conducted by Vital-Reyes et al., utilize Ki-67 to check for proliferation arrest and cellular growth pre and post-treatment, respectively [144]. In this study, we stained SKOV3 aggregates on day seven with Ki-67 (magenta) and DAPI (blue) to indicate that the nuclei are in an active phase of the cell-cycle (Fig. 4.10).

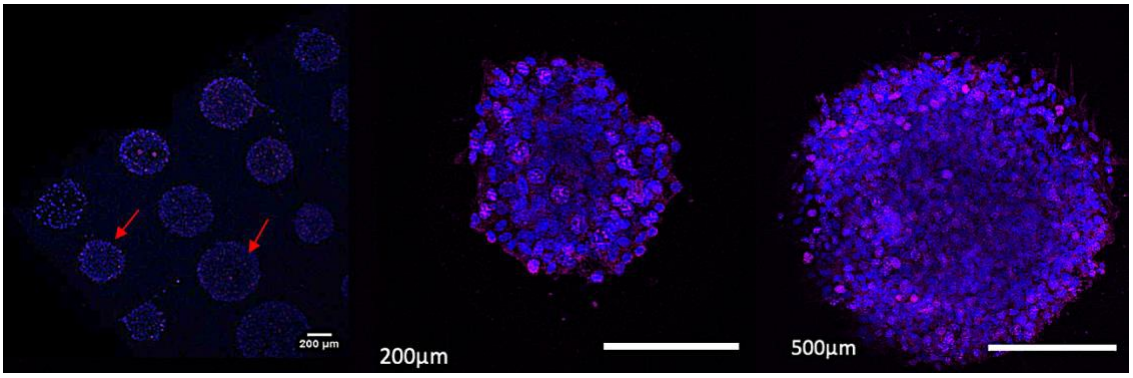

Figure 4.10: Proliferation biomarker assessment of SKOV3 after seven days of culturing. Maximum intensity projection images generated from confocal z-stacks of SKOV3 aggregates on a circle pattern stained for nuclei (DAPI, blue) and Ki-67 (magenta) at 4x and 20x. (scale 200 µm).

4.3.4 Polyploid "Giant" Cells

Interestingly, the appearance of giant cells was observed in both cell lines, however, it occurred more frequently in OVCAR3 cell cultures (Fig. 4.11). These cells were seen on the TiB_2 micropattern and had much larger nuclei, relative to the other surrounding cells. These cells also had a large clear space around them. Visual comparison of the biomarker Ki-67 on SKOV3 exhibiting giant cells showed that overall there are fewer nuclei expressing Ki-67. However, those nuclei show intensive staining, with the greatest saturation being in the giant cell nuclei (Fig. 4.11).

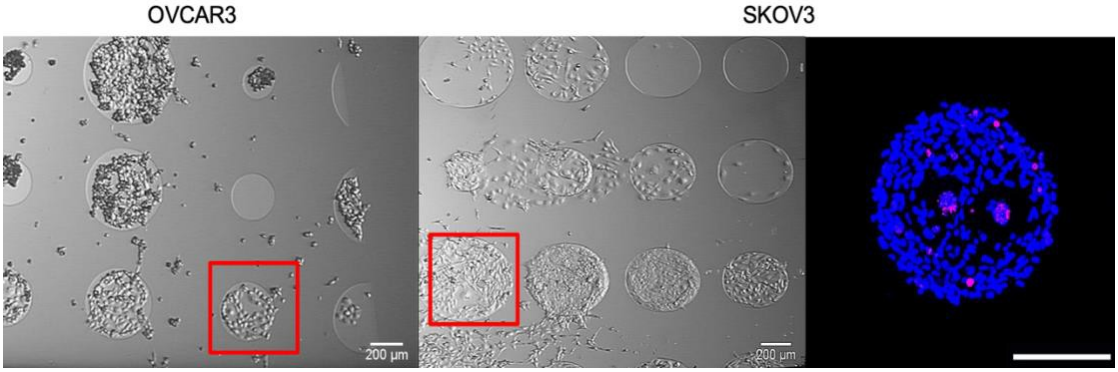

Figure 4.11: OVCAR3 and SKOV3 growth on the Si-TiB_2 micropatterned substrate. Representative reflected light images from stereomicroscopy Giant cells emphasized with red boxes. Maximum intensity projection image generated from confocal z-stacks of SKOV3 showing two mega (scale 200 µm).

It is plausible that these cells may have the phenotype of the polyploid giant cancer cells described by Niu et al. 2016 [135,145]. Interestingly, when SKOV3 exhibited giant cells, the aggregate formation was disrupted. Studies have reported that accelerated senescence is associated with the formation of polyploid giant cancer cells; since they possess the potential to form para-diploid progeny [144,146]. Zhang et al. and Niu et al.'s reported this phenomenon when looking further at genomic reorganization and generation of "cancer stem cells" [83,147,148].

4.4 Non-specific Growth in Cancer Cells During Extended Culture

OVCAR3 cells did not form well-defined aggregates over a seven-day culturing period and exhibited an initial preference to TiB_2 but then migrated to the Si background at 7 days. This is in-line with recent studies that have come out in support of the hypothesis that certain OvCa cell lines, such as (OVCAR3) are demonstrating more aggressive behavior, which is typically associated with High-Grade Serous cell lines. This aggressive behavior is linked to EMT, which is typically captured through an increase in the expression of mesenchymal proteins such as Vimentin [83,84,149]. Thus, to assess the adaptation of functional mesenchymal phenotype following migration onto the Si background, immunofluorescence staining for Vimentin on OVCAR3 was undertaken. The cells were counterstained with DAPI to visualize all cell nuclei.

In the case of OVCAR3, it was observed that on the outer edges of the TiB_2 circular patterns, and on cells that have migrated to the Si background, vimentin was highly expressed compared to the cells on the inner section of the circular patterns. Moreover, when SKOV3 aggregates were cultured for an additional seven days after the 3D aggregates had formed, sporadic migration of SKOV3 cells permeated from the lower layer of the aggregate (Fig. 4.12). Like OVCAR3, immunofluorescence staining of the migrating SKOV3 showed higher expression for mesenchymal phenotype Vimentin when compared to the cells on the circular background (Fig. 4.12) [69,150,151].

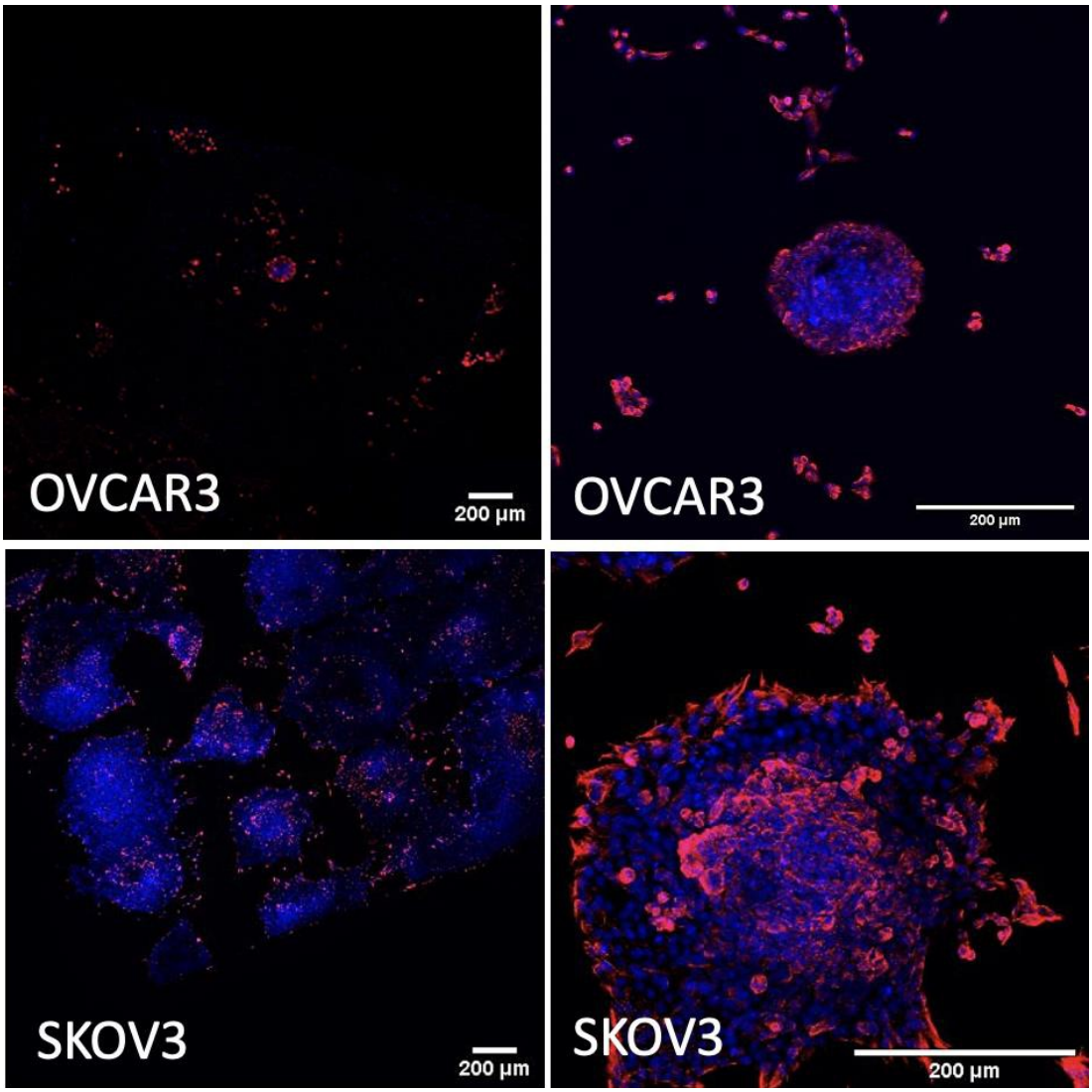

Figure 4.12: Mesenchymal biomarker assessment of SKOV3 and OVCAR3 after seven days of culturing. Maximum intensity projection images generated from confocal z-stacks of SKOV3 aggregates on a circle pattern stained for nuclei (DAPI, blue) and Vimentin (red) at 4x and 20x (scale 200 µm).

On our substrate, OVCAR3 and SKOV3's migration onto Si suggests a plausible role of stiffness gradients, which may be promoting cell migration due to a switch of a phenotype, which plays a complex role in the pathological and physiological process in cancer metastasis [152].

4.5 Effect of SAHA on SKOV3 Aggregates

SAHA's potential epigenomic disruption effects on SKOV3 aggregates was assessed by treating day seven aggregates with 3 μM SAHA. Statistical analysis was performed for thickness, diameter, and viability using nine experiments with at least one data point for 200, 250, 300, 350, 400, 450, and 500 μm per experiment. We allowed the SKOV3 to culture and proliferate on the TiB_2 micropatterned substrates for a seven-day period until the formation of 3D aggregates, after which we introduced a sublethal dose of 3μM SAHA. The aggregates were assessed 48h after treatment.

Representative reflected light images from stereomicroscopy show a reduction of SKOV3 aggregate size at day nine after the introduction of 3μM SAHA on day seven (Fig. 4.13). The thickness of said aggregates reduced from 50 μm for untreated aggregates to 35 μm for SAHA treated cells. The overall area of the aggregates decreased by 64%, while the volume decreased by 60% (Fig. 22). Additionally, the viability of the corresponding stereomicroscopy images is presented in Fig. 4.13 through a maximum intensity projection of AO/PI stained aggregates after culture in 3μM SAHA supplemented media.

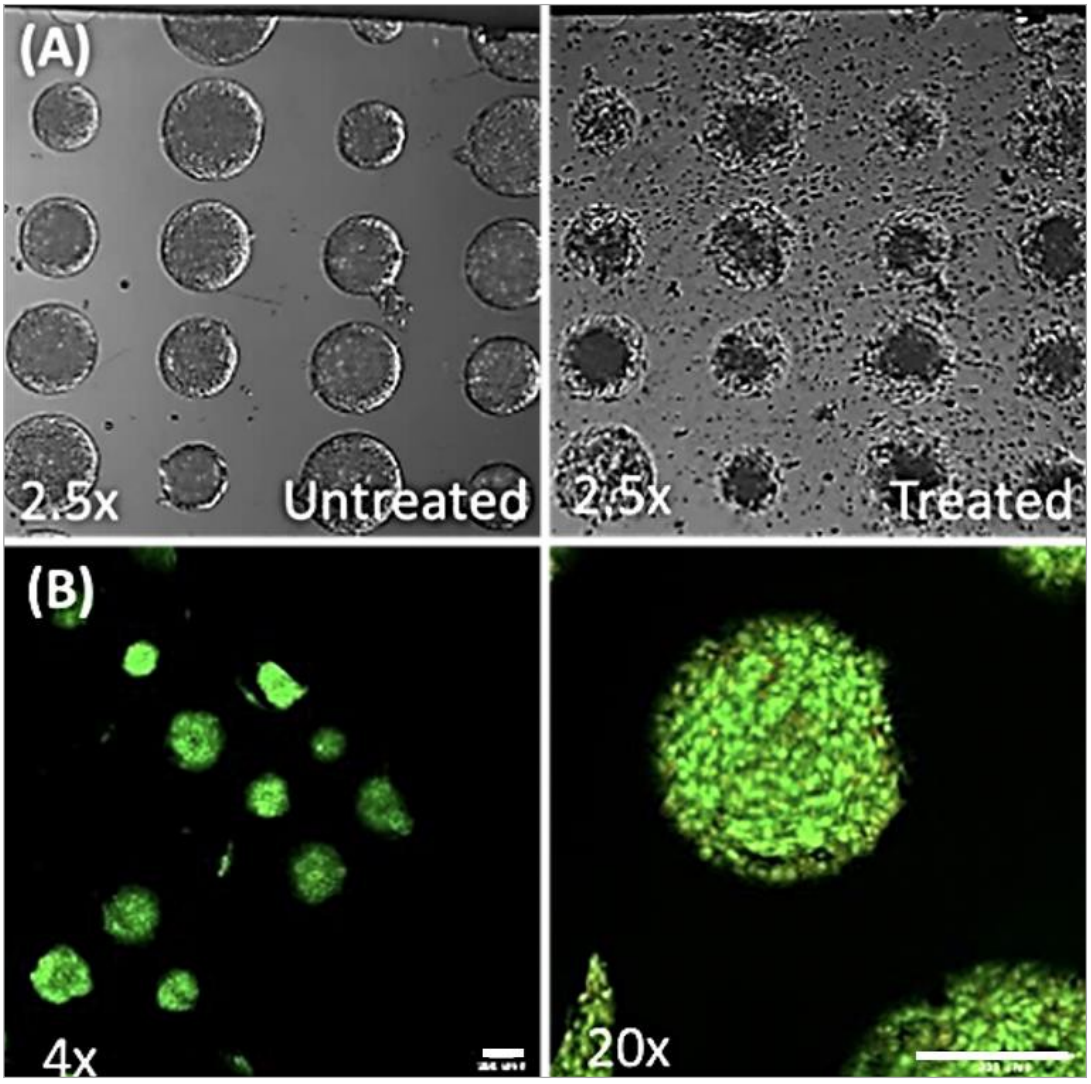

Figure 4.13: SKOV3 growth on the Si-TiB_2 micropatterned substrate. (A) The first column shows images of untreated SKOV3 and at 48h after introduction of 3μM SAHA (scale 100 μm). (B) Corresponding 4x and 20x objective maximum intensity projection generated from confocal z-stacks of SKOV3 3D aggregates at 48h after introduction of 3μM SAHA, stained for viability with Acridine Orange (green, live) and Propidium Iodide (red, dead).

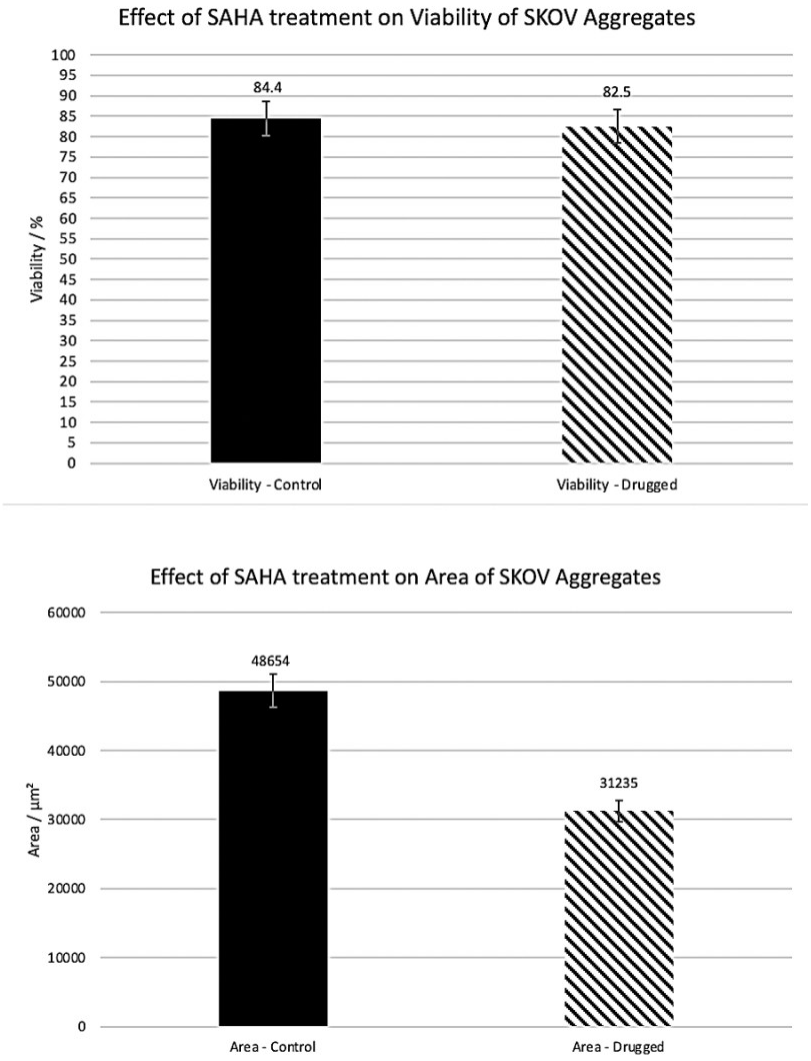

Figure 4.14: Plots of viability and area reduction after aggregates were treated with SAHA. Generated by PHStat on Excel.

We observed that the viability between the 3D aggregates treated with 3µM SAHA ranged from 80-85% with a mean value of 82% for treated, compared to 81-86% with a mean value of 83% for untreated. The thickness of said aggregates reduced from 50 µm for untreated aggregates to 35 µm for SAHA treated cells, and the overall calculated volume showed a reduction by 60%. Moreover, the area of the aggregates decreased from 48.7×10^3 µm^2 to 31.2×10^3 µm^2 after treatment (Fig. 4.14).

4.5.1 Fate of Detached Cells Following SAHA Treatment

Media from SAHA treated aggregates was collected and re-plated to assess their ability to proliferate. At 48 h after treatment with SAHA, the media was re-plated on MaTek dishes. The results show that the cells that dissociated from the 3D aggregates remained viable (Fig. 4.15) but proliferated less than cells that dissociated from nontreated aggregates (Fig. 24). Additional microscopy images of re-plated media collected from treated aggregates suggest slow proliferation throughout a seven-day period. Assessment of proliferation marker; Ki-67, along with cytoskeleton marker (F-actin), demonstrated the plated cells were not in a proliferation state and contained a population of elongated and cobblestone cells (Fig. 4.15) [86,153–155].

We proposed that these cells might be experiencing anoikis resistance and proliferation arrest as they seem to be able to re-attach to the MaTek dishes and survive, without growing any further [154]. This is similar to what was seen by Kim et al. when looking into OvCa tumor progression and molecular pathways. Their study was a cross-sectional review that described the findings of all current investigations into cellular mechanisms, including senescence. They found that anoikis is an essential part of normal cell development that avoids dysplasticity. However, cancerous cells thrive and spread due to anoikis resistance, which aids in metastasis and dissemination [143].

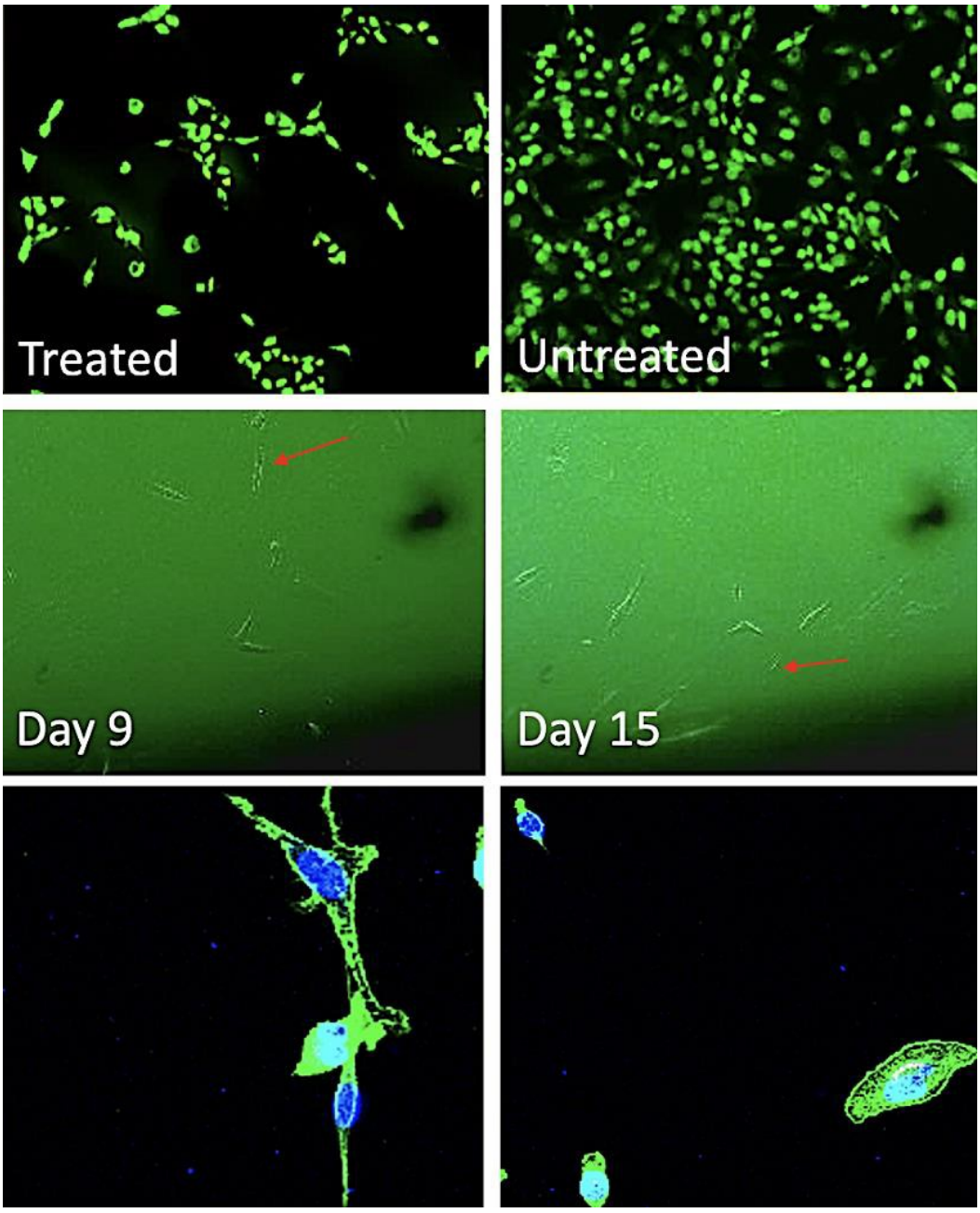

Figure 4.15: Effect of SAHA on SKOV3 growth on the Si-TiB_2 micropatterned substrate. Media was collected from SKOV3 3D aggregates after nine days and re-plated for 48h for both treated and untreated aggregates. The top right panel contains corresponding maximum intensity projection images generated from confocal z-stacks of both treated and untreated SKOV3 stained for viability with Acridine Orange (green, live) and Propidium Iodide (red, dead). Below it contains microscopy images of treated cells on day nine and fifteen. Finally, the bottom row contains corresponding maximum intensity projection images generated from confocal z-stacks of the same microscopy images in the row above it stained with F-actin (green), Ki-67 (magenta), and DAPI (blue) [Red arrows indicate corresponding cells shown in the row below].

4.5.2 Biomarker Assessment in Cells Treated with SAHA

Vimentin is typically associated with EMT transition and stem-like histochemistry, whilst Ki-67 is seen as an indicator of increased proliferation (often in HGS spheroids) as seen by Burford et al. when quantifying the effect of chemotherapy on cell proliferation and stemness [61,156].

Although SAHA did not impact the viability of SKOV3, additional phenotypic assessments were conducted after 48h of treatment. Through immunofluorescence evaluation of mesenchymal phenotype (Vimentin) and proliferation (Ki-67) properties, it is shown that SAHA not only reduces the SKOV3 spheroid volume, it also suppresses the expression of vimentin in the remaining aggregate (Fig. 4.16).

Moreover, preliminary results suggest no visually apparent change in expression of Ki-67 when compared to the untreated aggregate (Fig. 4.16). However, treated aggregates showed Ki-67 concentrated within fewer nuclei. In order to make it easier to differentiate the stains, we used yellow instead of magenta for Ki-67.

Additional repeats are necessary, as well as RNA analysis, in order to validate and quantify the effect of SAHA treatment on proliferation and mesenchymal biomarkers.

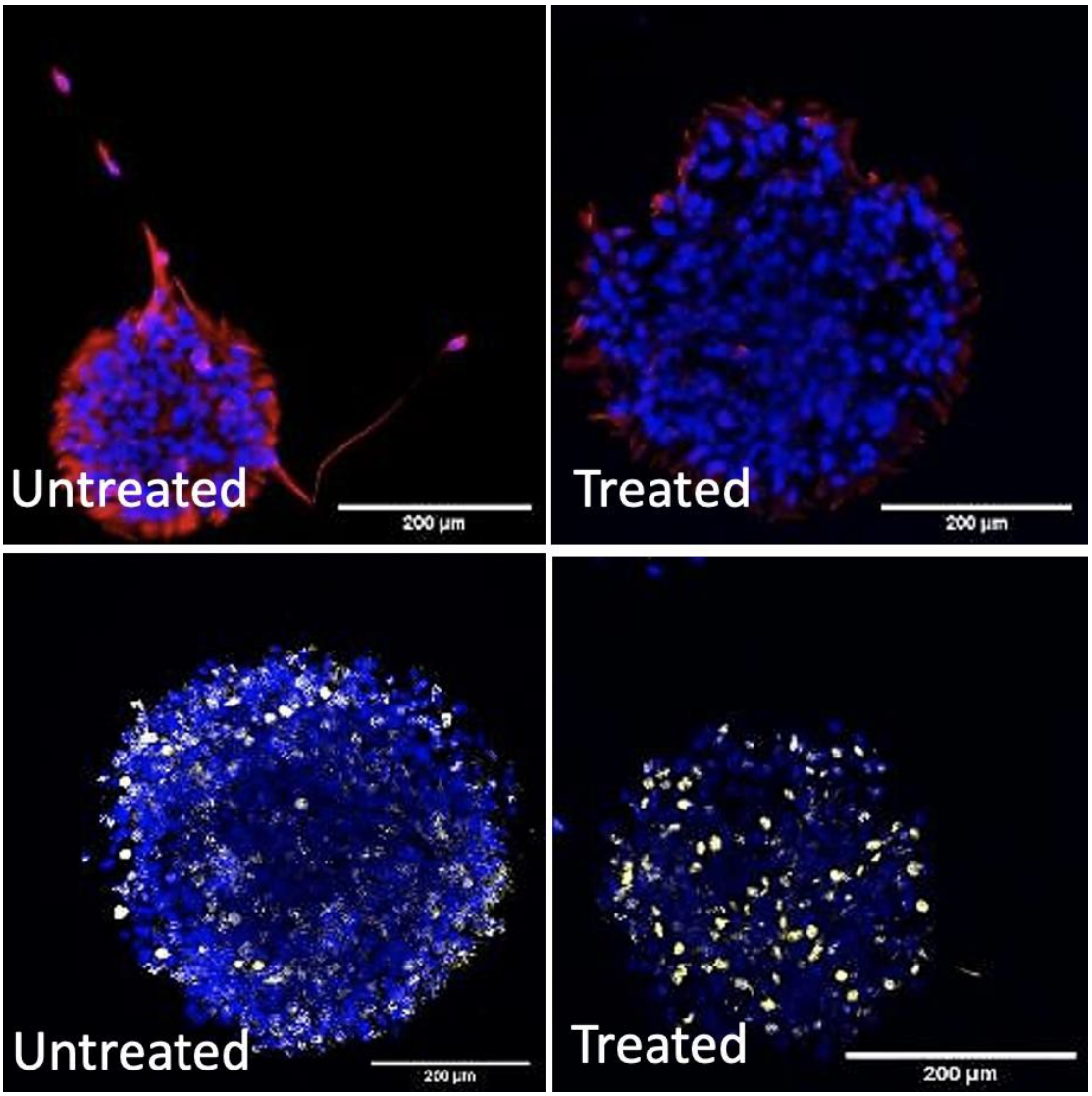

Figure 4.16: Morphological and biomarker assessment of drug-treated and untreated SKOV3 after one-week of culturing. The top panel contains maximum intensity projection images generated from confocal z-stacks of untreated and treated SKOV3 aggregates on a circle pattern stained for nuclei (blue) and vimentin (red), the row below it contains nuclei (blue) and Ki-67 (yellow) to assess the impact of SAHA on SKOV3 phenotype (scale 200µm).

CHAPTER 5 CONCLUSION AND DISCUSSION

Unlike most cancerous malignancies, metastasis of epithelial ovarian cancer (OvCa) occurs primarily via dissemination. This is characterized by shedding of cells from the primary tumor, avoidance of anoikis, movement throughout the peritoneal cavity as individual cells and spheroidal aggregates, adhesion to and disruption of the mesothelial lining of the peritoneum, and proliferation to generate widely disseminated metastases. With very little improvement in testing methods and more struggles in addressing drug treatment of OvCa, more needs to be done to develop a better 3D platform to optimize OvCa cellular functions, growth, and drug response.

This study demonstrated the successful utilization of a novel micropatterned Si-TiB_2 substrate for the investigation of Ovarian Cancer (OvCa) aggregate formation, as well as the effect of deacetylase histone inhibitor SAHA on the stability of OvCa aggregates. In this regard, we have shown the potential of the biomaterials, Si and TiB_2 in tissue culture applications for the assessment of cancer cells.

OvCa cells sense their mechanical environment, by exerting a contractile force and sensing the subsequent counter-tension through their cell membranes and cytoskeletons [9,10,157,158]. OvCa tumors are often surrounded with stiffened, fibrotic tissue, with an upregulation in ECM proteins and components. Furthermore, studies directly link contractility to increasing matrix stiffness and subsequent cancer progression. An increase in substrate stiffness has been demonstrated to increase oncogenic proliferation, migration, stemness, and chemoresistance [49,51,52,159].

In this study, with the Si-TiB_2 substrate, the Si background is less stiff compared to TiB_2, thus a stiffness gradient is established across the TiB_2 patterns and the Si

background. This made it more suitable for cellular attachment and growth, which has been the main hurdle for most 3D culture techniques; as is seen in cross-sectional 3D assessment studies [51,52,54]. Roughness differences between TiB_2 and Si provide an additional differential property, providing easier attachment of cells to the TiB_2 compared to the Si background.

Upon observation and documentation of SKOV3 and OVCAR3 cultures on the substrates, OvCa cells proliferated and remained viable, for the duration of the experiment (approximately seven days). They also retained their characteristic morphology whether it was spindle-shaped or round, without displaying stress or death; with a viability factor that matches most 3D culture systems at 83% [62,133,160–162]. SKOV3 formed 3D aggregates on TiB_2 micropatterns, while the same could not be said for OVCAR3, which is corroborated by other studies demonstrating OVCAR3's lack of aggregation [5,6,52,163]. OVCAR3 also lost specific adherence to the circular patterns sooner, while SKOV3 responded more dramatically to surface differences by maintaining its specific adherence to the circular TiB_2 patterns, eventually forming 3D aggregates by day seven. Due to this difficulty of forming OVCAR3 aggregates, SKOV3 was seen as a more ideal choice for studying the effects of epigenetic drugs.

SKOV3 aggregates typically fell within a high range of viability, with the majority of aggregates demonstrating a viability of greater than 80% with an overall average viability of 83%. Aggregates also typically formed to generate a depth of roughly 45-55 μm, sometimes ranging to be as large as 80 μm in depth. Aggregate diameters fluctuated based on micropattern diameter, ranging from 120-490 μm. Therefore, suggesting that the aggregates formed are biologically relevant in terms of

size, since OvCa spheroids captured in vivo appear to range from 50-750 μm in diameter. Furthermore, *in vivo* spheroids also demonstrate a high degree of viability, similar to the aggregates formed on TiB_2 substrate [53,164]. Some studies, including Raghavan et al. and Paradiso et al., using ultra-low attachment (ULA) plates, Matrigel, and even marine collagen report spheroids 30–100 μm with viability between 75-85% [5,6,52,54,116,163,165]. These dimensions put this platform at the forefront of cutting-edge technology that captures realistic and translational 3D aggregate formation, especially when compared to other 3D models on the market. Although other models can capture short-term molecular changes within cells, providing a useful snapshot of the disease progression, low stiffness, limited long-term stability, and batch-to-batch variability limits these kinds of 3D spheroid culturing techniques [48,49,53,159].

3D microenvironments that capture a more realistic image of OvCa's life cycle in vitro, are necessitated for experimentation. The main disadvantage of even the leading 2D monolayer cultures is often ineffectiveness at predicting drug efficacy in vivo [147]. SKOV3 is a metastatic cell line with high invasive potential and in our studies, with the micropatterned substrate, it was observed to be susceptible to EMT. This aligns with previously established studies, by Klymenko et al. demonstrated that cells adopting a mesenchymal phenotype show strong cell-cell adhesions and are more efficient in invading and seeding the intraperitoneal space. SKOV3 showed features similar to an early dissemination step in OvCa such as expression of the mesenchymal marker vimentin [57,62,161].

OVCAR3 has historically been deemed an OvCa cell line with low invasive potential [5,166–168]. Strangely, we observed that on the outer edges of the TiB_2

circular patterns, and on cells that have migrated to the Si background, Vimentin was highly expressed compared to the cells on the inner section of the circular patterns in OVCAR3 cultures. This aligns with more recent studies emerging in support of relabeling OVCAR3 as HGS or a metastatic and invasive cell line exhibiting EMT properties [169]. Certain OVCAR3 cell lines formed intraperitoneal tumors with HGS histology and gave rise to subcutaneous xenografts that invaded more aggressively once they were able to migrate as seen by Hallas-Potts et al. [58,79,152,161]. However, since confirmation of EMT (and even MET) requires reporting levels of the transcription factors ZEB, Snail, and Twist and the expression/lack of expression of epithelial markers [99], further immunofluorescence staining and RNA analysis should be pursued for both cell lines.

As for assessing the platform for drug treatment, Suberoylanilide Hydroxamic acid (SAHA) was used to create epigenomic disruption [99,170]. SAHA induced a decrease in the thickness of SKOV3 aggregates by approximately 60%. That is to be expected as SAHA is typically associated with dissemination, apoptosis, and reduction of invasive characteristics, such as migration, in SKOV3 [103,171]. SAHA has demonstrated clinical efficacy in the treatment of various hematological malignancies and is generally well tolerated such as Zhu et al.'s GI study and Kalanxhi et al.'s pelvis study [41,100,102,103]. However, when comparing the viabilities of treated and untreated SKOV3 aggregates, both were within a mean of 80-85%. Thus, despite high tolerability and significant effects on aggregation, individual therapy with SAHA only for the treatment of OvCa has demonstrated limited efficacy, and their ultimate usage clinically may be derived from combination treatments [102].

In this study, we observed SKOV3 aggregates shrinking and disaggregating, upon administering the SAHA treatment, without an overall reduction in viability. This is consistent with other findings, which demonstrate SAHA as not being particularly cytotoxic as a single agent treatment [103]. Zhu et al. conducted a combination drug treatment with Quinacrine and SAHA on GI cancers and noted that apoptosis was optimized in combination therapy as SAHA promoted disaggregation [100]. Alternatively, Liu et al. conducted a study comparing SAHA to the more common form of OvCa chemotherapy, Paclitaxel, then compared those to OvCA cells under a combined treatment [155]. They also observed that the disaggregation, prompted by SAHA and the induction of anoikis, allows for even the most chemo-resistant OvCa to become susceptible to apoptosis by Paclitaxel.

Even the disaggregated cells, which were re-plated on MaTek dishes, were viable signifying an ability to overcome anoikis. However, these detached cells did not proliferate after an additional seven-day culture and may therefore be senescent or in a state of proliferation arrest. As senescence and proliferation arrest are desirable outcomes of chemotherapeutic treatment, and general cancer treatment such as what is extensively documented by Liu et al. [41,100,103], these findings may further point towards the use of SAHA as a combination treatment, such as what is observed in decitabine, paclitaxel, and quinacrine experiments [99,170]. These combination treatments generally result in an increased expression of pro-apoptotic markers, as well as a decrease in surviving cells, which could compensate for SAHA's inability to directly affect viability [44,172,173].

From cell line adhesion to proliferation, dimensions, and the ability to capture induced epigenomic disturbances, I believe our proposed platform and method of culturing shows great potential in the field. This highlights a dual relevance in OvCa metastasis, which can be encapsulated by Si-TiB_2 substrate; the formation of a primary tumor spheroid, and secondly, the disruption of spheroids using epigenomic dysregulation. Additionally, the substrate allows for an investigation unique expression of mesenchymal biomarker vimentin, as both OVCAR3 and SKOV3 showed elevated expression on Si. Further research and characterization of the platform would aid in providing an even more robust system. Using the adjustable substrate to create an ideal environment for such studies has the potential to revolutionize how 3D culturing of cancer cells is done, thus, helping physicians and scientists in their pursuit. Hopefully, we will contribute towards reducing the high mortality associated with Ovarian Cancer.

CHAPTER 6 FUTURE WORK

Due to promising results with SKOV3 and OVCAR3, this work could be expanded to other OvCa cell lines. In addition to looking at new cell lines, further work could be carried out to characterize the effects of epigenomic disruption better. This could include combination therapies with SAHA or other epigenetic treatments, such as the methylation inhibitor, 5-aza [174–177]. Additionally, the platform could be used to observe if SAHA is providing a potentiating effect to treatment with chemotherapeutics such as paclitaxel or cisplatin since SAHA appears to be diminishing the 3D structure of aggregates.

Future work needs to also focus on the proposed polyploid giant cells sporadically shown in SKOV3 cultures. When SKOV3 exhibited these giant cells, the aggregate formation was disrupted, which was confirmed by Ki-67 IF staining, indicating accelerated senescence and potential para-diploid progeny dispersion [178–180]. This could feed into further EMT studies and genomic reorganization of OvCa metastatic tumors.

Lastly, additional RNA analysis needs to be conducted on SKOV3 and OVCAR3. Stemness markers including SOX17, SOX2, VEGFR2/KDR, HNF-3β/FOXA2, PDX-1/IPF1, Snail, and E-cadherin must be shown to be expressed at a significant level in either OVCAR3 or SKOV3 cell line in aggregates in contrast to migrating cells' expression levels [128,181]. Furthermore, RNA analysis can be utilized to see the effects of EMT inducing factors, such as KLF-4, and the fluctuations in expression levels in the case of adverse effects of chemotherapy [128,181].

REFERENCES

1. Weatherspoon D, Timmons J. Ovarian Cancer: Facts, Statistics, and You. https://www.healthline.com/health/cancer/ovarian-cancer-facts-statistics-infographic. 2019.
2. Types & Stages of Ovarian Cancer. https://www.ovarian.org/about-ovarian-cancer/what-is-ovarian-cancer/types-a-stages.
3. Survival Comparison Statistical Methodology. https://www.cancercenter.com/become-a-patient/our-treatment-results/survival-statistics-and-results/statistical-methodology.
4. World Ovarian Cancer Coalition - Atlas. https://worldovariancancercoalition.org/.
5. Jones PM, Drapkin R. Modeling High-Grade Serous Carcinoma: How Converging Insights into Pathogenesis and Genetics are Driving Better Experimental Platforms. Frontiers in Oncology. 2013;3.
6. Bielecka ZF, Maliszewska-Olejniczak K, Safir IJ, Szczylik C, Czarnecka AM. Three-dimensional cell culture model utilization in cancer stem cell research. Biological Reviews. 2017 Aug;92(3).
7. White EA, Kenny HA, Lengyel E. Three-dimensional modeling of ovarian cancer. Advanced Drug Delivery Reviews. 2014 Dec;79–80.
8. Kerkar SP, Restifo NP. Cellular Constituents of Immune Escape within the Tumor Microenvironment. Cancer Research. 2012 Jul 1;72(13).
9. Samuel MS, Lopez JI, McGhee EJ, Croft DR, Strachan D, Timpson P, et al. Actomyosin-Mediated Cellular Tension Drives Increased Tissue Stiffness and β-Catenin Activation to Induce Epidermal Hyperplasia and Tumor Growth. Cancer Cell. 2011 Jun;19(6).
10. Wormer DB, Davis KA, Henderson JH, Turner CE. The Focal Adhesion-Localized CdGAP Regulates Matrix Rigidity Sensing and Durotaxis. PLoS ONE. 2014 Mar 14;9(3).
11. Friedl P, Alexander S. Cancer Invasion and the Microenvironment: Plasticity and Reciprocity. Cell. 2011 Nov;147(5).
12. Loret N, Denys H, Tummers P, Berx G. The Role of Epithelial-to-Mesenchymal Plasticity in Ovarian Cancer Progression and Therapy Resistance. Cancers. 2019 Jun 17;11(6).
13. Qiu L, Burgess A, Fairlie DP, Leonard H, Parsons PG, Gabrielli BG. Histone Deacetylase Inhibitors Trigger a G2 Checkpoint in Normal Cells That Is Defective in Tumor Cells. Molecular Biology of the Cell. 2000 Jun;11(6).
14. Marks PA. Histone deacetylase inhibitors: A chemical genetics approach to understanding cellular functions. Biochimica et Biophysica Acta (BBA) - Gene Regulatory Mechanisms. 2010 Oct;1799(10–12).
15. Kurman RJ, Shih I-M. The Origin and Pathogenesis of Epithelial Ovarian Cancer: A Proposed Unifying Theory. The American Journal of Surgical Pathology. 2010 Mar;34(3).

16. Kurman RJ, Shih I-M. The Dualistic Model of Ovarian Carcinogenesis. The American Journal of Pathology. 2016 Apr;186(4).
17. Sarosiek K. Searching for the ovarian cancer cell of origin. Science Translational Medicine. 2017 Nov 1;9(414).
18. Jemal A, Siegel R, Xu J, Ward E. Cancer Statistics, 2010. CA: A Cancer Journal for Clinicians. 2010 Sep 1;60(5).
19. Ovarian cancer. Silent and deadly | Atlas of Science. https://atlasofscience.org/ovarian-cancer-silent-and-deadly/ .
20. al Habyan S, Kalos C, Szymborski J, McCaffrey L. Multicellular detachment generates metastatic spheroids during intra-abdominal dissemination in epithelial ovarian cancer. Oncogene. 2018 Sep 23;37(37).
21. Visintin I, Feng Z, Longton G, Ward DC, Alvero AB, Lai Y, et al. Diagnostic Markers for Early Detection of Ovarian Cancer. Clinical Cancer Research. 2008 Feb 15;14(4).
22. Sorscher S. Understanding the Significance of Mutations in Tumor Suppressor Genes Identified Using Next-Generation Sequencing: A Case Report. Case Reports in Oncology. 2016 Jun 14;9(2).
23. Rådestad E, Klynning C, Stikvoort A, Mogensen O, Nava S, Magalhaes I, et al. Immune profiling and identification of prognostic immune-related risk factors in human ovarian cancer. OncoImmunology. 2019 Feb 16;8(2).
24. Cardenas C, Alvero AB, Yun BS, Mor G. Redefining the origin and evolution of ovarian cancer: a hormonal connection. Endocrine-Related Cancer. 2016 Sep;23(9).
25. Isabelle Matte, Denis Lane, Claude Laplante, Claudine Rancourt, Alain Piché. Profiling of cytokines in human epithelial ovarian cancer ascites. American Journal of Cancer Research. 2012;2(5):566–80.
26. Peng W, Liu C, Xu C, Lou Y, Chen J, Yang Y, et al. PD-1 blockade enhances T-cell migration to tumors by elevating IFN-γ inducible chemokines. Cancer Research. 2012 Oct 15;72(20):5209–18.
27. Rauh-Hain JA, Krivak TC, del Carmen MG, Olawaiye AB. Ovarian cancer screening and early detection in the general population. Reviews in obstetrics & gynecology [Internet]. 2011;4(1):15–21. Available from: https://pubmed.ncbi.nlm.nih.gov/21629494
28. Lengyel E. Ovarian Cancer Development and Metastasis. The American Journal of Pathology. 2010 Sep;177(3).
29. Modugno F, Edwards RP. Ovarian Cancer: Prevention, Detection, and Treatment of the Disease and its Recurrence. Molecular Mechanisms and Personalized Medicine Meeting Report. International Journal of Gynecologic Cancer. 2012 Oct 1;22(Supp 2).
30. Patni R. Screening for ovarian cancer: An update. Journal of Mid-life Health. 2019;10(1).
31. Bevers TB, Brown PH, Maresso KC, Hawk ET. Cancer Prevention, Screening, and Early Detection. In: Abeloff's Clinical Oncology. Elsevier; 2014.
32. About Ovarian Cancer. https://www.cancer.org/cancer/ovarian-cancer.html.

33. Ovarian Cancer: What is it? https://www.acog.org/womens-health/faqs/ovarian-cancer.
34. Cristea M, Han E, Salmon L, Morgan RJ. Review: Practical considerations in ovarian cancer chemotherapy. Therapeutic Advances in Medical Oncology. 2010 May 12;2(3).
35. Mikuła-Pietrasik J, Uruski P, Tykarski A, Książek K. The peritoneal "soil" for a cancerous "seed": a comprehensive review of the pathogenesis of intraperitoneal cancer metastases. Cellular and Molecular Life Sciences. 2018 Feb 27;75(3).
36. D'Alterio C, Scala S, Sozzi G, Roz L, Bertolini G. Paradoxical effects of chemotherapy on tumor relapse and metastasis promotion. Seminars in Cancer Biology. 2020 Feb;60.
37. Fields EC, McGuire WP, Lin L, Temkin SM. Radiation Treatment in Women with Ovarian Cancer: Past, Present, and Future. Frontiers in Oncology. 2017 Aug 21;7.
38. Sandercock J, Parmar MKB, Torri V, Qian W. First-line treatment for advanced ovarian cancer: paclitaxel, platinum and the evidence. British Journal of Cancer. 2002 Oct 7;87(8).
39. Lee J, Minasian L, Kohn EC. New strategies in ovarian cancer treatment. Cancer. 2019 Dec 15;125(S24).
40. Chandra A, Pius C, Nabeel M, Nair M, Vishwanatha JK, Ahmad S, et al. Ovarian cancer: Current status and strategies for improving therapeutic outcomes. Cancer Medicine. 2019 Nov 27;8(16).
41. Han T, Zhuo M, Hu H, Jiao F, Wang L-W. Synergistic effects of the combination of 5-Aza CdR and suberoylanilide hydroxamic acid on the anticancer property of pancreatic cancer. Oncology Reports. 2017 Oct 31;
42. Stone ML, Chiappinelli KB, Li H, Murphy LM, Travers ME, Topper MJ, et al. Epigenetic therapy activates type I interferon signaling in murine ovarian cancer to reduce immunosuppression and tumor burden. Proceedings of the National Academy of Sciences of the United States of America. 2017 Dec 19;114(51):E10981–90.
43. Yang C, Xia B-R, Zhang Z-C, Zhang Y-J, Lou G, Jin W-L. Immunotherapy for Ovarian Cancer: Adjuvant, Combination, and Neoadjuvant. Frontiers in Immunology. 2020 Oct 6;11.
44. Adair SJ, Hogan KT. Treatment of ovarian cancer cell lines with 5-aza-2′-deoxycytidine upregulates the expression of cancer-testis antigens and class I major histocompatibility complex-encoded molecules. Cancer Immunology, Immunotherapy. 2009 Apr 13;58(4).
45. Ushijima K. Treatment for Recurrent Ovarian Cancer—At First Relapse. Journal of Oncology. 2010;2010.
46. Colombo N, Lorusso D, Scollo P. Impact of Recurrence of Ovarian Cancer on Quality of Life and Outlook for the Future. International Journal of Gynecologic Cancer. 2017 Jul 1;27(6).

47. Miyoshi A, Kanao S, Naoi H, Otsuka H, Yokoi T. Ovarian Cancer: Post-Relapse Survival and Prognostic Factors. Journal of Clinical Gynecology and Obstetrics. 2018;7(2).
48. Duval K, Grover H, Han L-H, Mou Y, Pegoraro AF, Fredberg J, et al. Modeling Physiological Events in 2D vs. 3D Cell Culture. Physiology. 2017 Jul;32(4).
49. Kapałczyńska M, Kolenda T, Przybyła W, Zajączkowska M, Teresiak A, Filas V, et al. 2D and 3D cell cultures – a comparison of different types of cancer cell cultures. Archives of Medical Science. 2018;14(4):910–9.
50. Cho A, Howell VM, Colvin EK. The Extracellular Matrix in Epithelial Ovarian Cancer – A Piece of a Puzzle. Frontiers in Oncology. 2015 Nov 2;5.
51. Watters KM, Bajwa P, Kenny HA. Organotypic 3D Models of the Ovarian Cancer Tumor Microenvironment. Cancers. 2018 Aug 9;10(8).
52. Zhang C, Yang Z, Dong D-L, Jang T-S, Knowles JC, Kim H-W, et al. 3D culture technologies of cancer stem cells: promising ex vivo tumor models. Journal of Tissue Engineering. 2020 Jan 24;11.
53. Paradiso F, Fitzgerald J, Yao S, Barry F, Taraballi F, Gonzalez D, et al. Marine Collagen Substrates for 2D and 3D Ovarian Cancer Cell Systems. Frontiers in Bioengineering and Biotechnology. 2019 Dec 13;7.
54. Unal DB, Caliari SR, Lampe KJ. 3D Hyaluronic Acid Hydrogels for Modeling Oligodendrocyte Progenitor Cell Behavior as a Function of Matrix Stiffness. Biomacromolecules. 2020 Oct 28.
55. McKenzie AJ, Hicks SR, Svec K v., Naughton H, Edmunds ZL, Howe AK. The mechanical microenvironment regulates ovarian cancer cell morphology, migration, and spheroid disaggregation. Scientific Reports. 2018 Dec 8;8(1).
56. Friguglietti J, Das S, Le P, Fraga D, Quintela M, Gazze SA, et al. Novel Silicon Titanium Diboride Micropatterned Substrates for Cellular Patterning. Biomaterials. 2020 Jun;244.
57. Beaufort CM, Helmijr JCA, Piskorz AM, Hoogstraat M, Ruigrok-Ritstier K, Besselink N, et al. Ovarian cancer cell line panel (OCCP): Clinical importance of in vitro morphological subtypes. PLoS ONE. 2014 Sep 17;9(9).
58. Paik ES, Kim JH, Kim T-J, Lee J-W, Kim B-G, Bae D-S, et al. Prognostic significance of normal-sized ovary in advanced serous epithelial ovarian cancer. Journal of Gynecologic Oncology. 2018;29(1).
59. Mohaghegh P, Rockall AG. Imaging Strategy for Early Ovarian Cancer: Characterization of Adnexal Masses with Conventional and Advanced Imaging Techniques. RadioGraphics. 2012 Oct;32(6).
60. Domcke S, Sinha R, Levine DA, Sander C, Schultz N. Evaluating cell lines as tumour models by comparison of genomic profiles. Nature Communications. 2013 Oct 9;4(1).
61. Weidle UH, Birzele F, Kollmorgen G, Rueger R. Mechanisms and targets involved in dissemination of ovarian cancer. Vol. 13, Cancer Genomics and Proteomics. International Institute of Anticancer Research; 2016. p. 407–24.
62. Sakhare SS, Rao GG, Mandape SN, Pratap S. Transcriptome profile of OVCAR3 cisplatin-resistant ovarian cancer cell line. BMC Bioinformatics. 2014;15(Suppl 10).

63. Bhattacharya R, Mitra T, Ray Chaudhuri S, Roy SS. Mesenchymal splice isoform of CD44 (CD44s) promotes EMT/invasion and imparts stem‐like properties to ovarian cancer cells. Journal of Cellular Biochemistry. 2018 Apr 4;119(4).
64. Ahmed N, Stenvers KL. Getting to Know Ovarian Cancer Ascites: Opportunities for Targeted Therapy-Based Translational Research. Frontiers in Oncology. 2013;3.
65. Shield K, Ackland ML, Ahmed N, Rice GE. Multicellular spheroids in ovarian cancer metastases: Biology and pathology. Gynecologic Oncology. 2009 Apr;113(1).
66. Raghavan S, Ward MR, Rowley KR, Wold RM, Takayama S, Buckanovich RJ, et al. Formation of stable small cell number three-dimensional ovarian cancer spheroids using hanging drop arrays for preclinical drug sensitivity assays. Gynecologic Oncology. 2015 Jul 1;138(1):181–9.
67. Symowicz J, Adley BP, Gleason KJ, Johnson JJ, Ghosh S, Fishman DA, et al. Engagement of Collagen-Binding Integrins Promotes Matrix Metalloproteinase-9–Dependent E-Cadherin Ectodomain Shedding in Ovarian Carcinoma Cells. Cancer Research. 2007 Mar 1;67(5).
68. Li Y, Kumacheva E. Applied Sciences and Engineering. Hydrogel microenvironments for cancer spheroid growth and drug screening [Internet]. 2018. Available from: http://advances.sciencemag.org/
69. Kalli M, Stylianopoulos T. Defining the Role of Solid Stress and Matrix Stiffness in Cancer Cell Proliferation and Metastasis. Frontiers in Oncology. 2018 Mar 12;8.
70. Ghoneum A, Afify H, Salih Z, Kelly M, Said N. Role of tumor microenvironment in ovarian cancer pathobiology. Oncotarget. 2018 Apr 27;9(32).
71. Kerkar SP, Restifo NP. Cellular Constituents of Immune Escape within the Tumor Microenvironment. Cancer Research. 2012 Jul 1;72(13).
72. Lane D, Matte I, Garde-Granger P, Bessette P, Piché A. Ascites IL-10 Promotes Ovarian Cancer Cell Migration. Cancer Microenvironment. 2018 Dec 23;11(2–3).
73. Gao Q, Yang Z, Xu S, Li X, Yang X, Jin P, et al. Heterotypic CAF-tumor spheroids promote early peritoneal metastasis of ovarian cancer. Journal of Experimental Medicine. 2019 Mar 4;216(3).
74. Cheng Y, He C, Wang M, Ma X, Mo F, Yang S, et al. Targeting epigenetic regulators for cancer therapy: mechanisms and advances in clinical trials. Signal Transduction and Targeted Therapy. 2019 Dec 17;4(1).
75. Gardner MJ, Catterall JB, Jones LMH, Turner GA. Human ovarian tumour cells can bind hyaluronic acid via membrane CD44: a possible step in peritoneal metastasis. Clinical & Experimental Metastasis. 1996 Sep;14(4).
76. Yeung T-L, Leung CS, Yip K-P, Au Yeung CL, Wong STC, Mok SC. Cellular and molecular processes in ovarian cancer metastasis. A Review in the Theme: Cell and Molecular Processes in Cancer Metastasis. American Journal of Physiology-Cell Physiology. 2015 Oct 1;309(7).

77. Bai, Zhu, Coffman, Vlad, Schwartz, Elishaev, et al. CD105 Is Expressed in Ovarian Cancer Precursor Lesions and Is Required for Metastasis to the Ovary. Cancers. 2019 Nov 2;11(11).
78. Kenny HA, Kaur S, Coussens LM, Lengyel E. The initial steps of ovarian cancer cell metastasis are mediated by MMP-2 cleavage of vitronectin and fibronectin. Journal of Clinical Investigation. 2008 Apr 1;118(4).
79. Sánchez-Tilló E, Liu Y, de Barrios O, Siles L, Fanlo L, Cuatrecasas M, et al. EMT-activating transcription factors in cancer: beyond EMT and tumor invasiveness. Cellular and Molecular Life Sciences. 2012 Oct 4;69(20).
80. Rohnalter V, Roth K, Finkernagel F, Adhikary T, Obert J, Dorzweiler K, et al. A multi-stage process including transient polyploidization and EMT precedes the emergence of chemoresistent ovarian carcinoma cells with a dedifferentiated and pro-inflammatory secretory phenotype. Oncotarget. 2015 Nov 24;6(37).
81. Liang W, Liu J, Wu H, Qiao X, Lu X, Liu Y, et al. Artemisinin induced reversal of EMT affects the molecular biological activity of ovarian cancer SKOV3 cell lines. Oncology Letters. 2019 Jul 11;
82. Strouhalova K, Přechová M, Gandalovičová A, Brábek J, Gregor M, Rosel D. Vimentin intermediate filaments as potential target for cancer treatment. Vol. 12, Cancers. MDPI AG; 2020.
83. Liu C-Y, Lin H-H, Tang M-J, Wang Y-K. Vimentin contributes to epithelial-mesenchymal transition cancer cell mechanics by mediating cytoskeletal organization and focal adhesion maturation. Oncotarget. 2015 Jun 30;6(18).
84. Kenda Suster N, Smrkolj S, Virant-Klun I. Putative stem cells and epithelial-mesenchymal transition revealed in sections of ovarian tumor in patients with serous ovarian carcinoma using immunohistochemistry for vimentin and pluripotency-related markers. Journal of Ovarian Research. 2017 Dec 23;10(1).
85. Peinado H, Alečković M, Lavotshkin S, Matei I, Costa-Silva B, Moreno-Bueno G, et al. Melanoma exosomes educate bone marrow progenitor cells toward a pro-metastatic phenotype through MET. Nature Medicine. 2012 Jun 27;18(6).
86. Paoli P, Giannoni E, Chiarugi P. Anoikis molecular pathways and its role in cancer progression. Biochimica et Biophysica Acta (BBA) - Molecular Cell Research. 2013 Dec;1833(12).
87. Shishido A, Mori S, Yokoyama Y, Hamada Y, Minami K, Qian Y, et al. Mesothelial cells facilitate cancer stem like properties in spheroids of ovarian cancer cells. Oncology Reports. 2018 Jul 27;
88. Gunay G, Kirit HA, Kamatar A, Baghdasaryan O, Hamsici S, Acar H. The effects of size and shape of the ovarian cancer spheroids on the drug resistance and migration. Gynecologic Oncology. 2020 Nov;159(2).
89. Gujar S, Dielschneider R, Clements D, Helson E, Shmulevitz M, Marcato P, et al. Multifaceted Therapeutic Targeting of Ovarian Peritoneal Carcinomatosis Through Virus-induced Immunomodulation. Molecular Therapy. 2013 Feb;21(2).
90. Moufarrij S, Dandapani M, Arthofer E, Gomez S, Srivastava A, Lopez-Acevedo M, et al. Epigenetic therapy for ovarian cancer: promise and progress. Clinical Epigenetics. 2019 Dec 15;11(1).

91. Yang Q, Yang Y, Zhou N, Tang K, Lau WB, Lau B, et al. Epigenetics in ovarian cancer: premise, properties, and perspectives. Molecular Cancer. 2018 Dec 31;17(1).
92. Smith HJ, Straughn JM, Buchsbaum DJ, Arend RC. Epigenetic therapy for the treatment of epithelial ovarian cancer: A clinical review. Gynecologic Oncology Reports. 2017 May;20.
93. Lakshminarasimhan R, Liang G. The Role of DNA Methylation in Cancer. In 2016.
94. Zhao M, Sun J, Zhao Z. Distinct and Competitive Regulatory Patterns of Tumor Suppressor Genes and Oncogenes in Ovarian Cancer. PLoS ONE. 2012 Aug 30;7(8).
95. Ungerstedt JS, Sowa Y, Xu W-S, Shao Y, Dokmanovic M, Perez G, et al. Role of thioredoxin in the response of normal and transformed cells to histone deacetylase inhibitors. Proceedings of the National Academy of Sciences. 2005 Jan 18;102(3).
96. Tang HM, Kuay KT, Koh PF, Asad M, Tan TZ, Chung VY, et al. An epithelial marker promoter induction screen identifies histone deacetylase inhibitors to restore epithelial differentiation and abolishes anchorage independence growth in cancers. Cell Death Discovery. 2016 Dec 13;2(1).
97. Marks PA, Breslow R. Dimethyl sulfoxide to vorinostat: development of this histone deacetylase inhibitor as an anticancer drug. Nature Biotechnology. 2007 Jan 8;25(1).
98. Mrakovcic M, Bohner L, Hanisch M, Fröhlich LF. Epigenetic Targeting of Autophagy via HDAC Inhibition in Tumor Cells: Role of p53. International Journal of Molecular Sciences. 2018 Dec 8;19(12).
99. Chen S, Zhao Y, Gou W, Zhao S, Takano Y, Zheng H. The Anti-Tumor Effects and Molecular Mechanisms of Suberoylanilide Hydroxamic Acid (SAHA) on the Aggressive Phenotypes of Ovarian Carcinoma Cells. PLoS ONE. 2013 Nov 13;8(11).
100. Liu Z, Tong Y, Liu Y, Liu H, Li C, Zhao Y, et al. Effects of suberoylanilide hydroxamic acid (SAHA) combined with paclitaxel (PTX) on paclitaxel-resistant ovarian cancer cells and insights into the underlying mechanisms. Cancer Cell International. 2014 Dec 26;14(1).
101. Chen M-Y, Liao WS-L, Lu Z, Bornmann WG, Hennessey V, Washington MN, et al. Decitabine and suberoylanilide hydroxamic acid (SAHA) inhibit growth of ovarian cancer cell lines and xenografts while inducing expression of imprinted tumor suppressor genes, apoptosis, G2/M arrest, and autophagy. Cancer. 2011 Oct 1;117(19).
102. Nolan L, Johnson PWM, Ganesan A, Packham G, Crabb SJ. Will histone deacetylase inhibitors require combination with other agents to fulfil their therapeutic potential? British Journal of Cancer. 2008 Sep 19;99(5).
103. Zhu S, Chen Z, Wang L, Peng D, Belkhiri A, Lockhart AC, et al. A Combination of SAHA and Quinacrine Is Effective in Inducing Cancer Cell Death in Upper Gastrointestinal Cancers. Clinical Cancer Research. 2018 Apr 15;24(8).

104. Gehrke P, Dinkel J, Fischer C, Schmenger K, Sader R. Surface Roughness and Necessity of Manual Refinishing Requirements of CAD/CAM-Manufactured Titanium and Cobalt-Chrome Bars – A Pilot Study. The Open Dentistry Journal. 2019 Aug 30;13(1).
105. Bhushan B. Surface Roughness Analysis and Measurement Techniques. Modern Tribology Handbook. 2000;1, 2:0–72.
106. McPhail D. Titanium diboride bioMEMS; investigating ovarian cancer spheroid formation in the presence of epigenomic instability. 2019.
107. Fiji/ImageJ.
108. Spivak-Kroizman T, Lemmon MA, Dikic I, Ladbury JE, Pinchasi D, Huang J, et al. Heparin-induced oligomerization of FGF molecules is responsible for FGF receptor dimerization, activation, and cell proliferation. Cell. 1994 Dec;79(6).
109. Levine A, Kenet G, Bruck R, Avni Y, Avinoach I, Aeed H, et al. Effect of Heparin on Tissue Binding Activity of Fibroblast Growth Factor and Heparin-Binding Epidermal Growth Factor in Experimental Colitis in Rats. Pediatric Research. 2002 May;51(5).
110. Haddad LE, Khzam LB, Hajjar F, Merhi Y, Sirois MG. Characterization of FGF receptor expression in human neutrophils and their contribution to chemotaxis. American Journal of Physiology-Cell Physiology. 2011 Nov;301(5).
111. Huang H-K, Lin Y-H, Chang H-A, Lai Y-S, Chen Y-C, Huang S-C, et al. Chemoresistant ovarian cancer enhances its migration abilities by increasing store-operated Ca2+ entry-mediated turnover of focal adhesions. Journal of Biomedical Science. 2020 Dec 21;27(1).
112. Chandler LA, Sosnowski BA, Greenlees L, Aukerman SL, Baird A, Pierce GF. Prevalent expression of fibroblast growth factor (FGF) receptors and FGF2 in human tumor cell lines. International Journal of Cancer. 1999 May 5;81(3).
113. Huang H-H, Ho C-T, Lee T-H, Lee T-L, Liao K-K, Chen F-L. Effect ofsurface roughness of ground titanium on initial cell adhesion. Biomolecular Engineering. 2004 Nov;21(3–5).
114. Mutreja I, Ye Z, Aparicio C. Cell responses to titanium and titanium alloys. In: Handbook of Biomaterials Biocompatibility. Elsevier; 2020.
115. Shiozawa M, Takeuchi H, Akiba Y, Eguchi K, Akiba N, Aoyagi Y, et al. Biological reaction control using topography regulation of nanostructured titanium. Scientific Reports. 2020 Dec 12;10(1).
116. Heredia-Soto V, Redondo A, Berjón A, Miguel-Martín M, Díaz E, Crespo R, et al. High-throughput 3-dimensional culture of epithelial ovarian cancer cells as preclinical model of disease. Oncotarget. 2018 Apr 24;9(31).
117. Hanna EA. Gap junctional intercellular communication and connexin43 expression in human ovarian surface epithelial cells and ovarian carcinomas in vivo and in vitro. Carcinogenesis. 1999 Jul 1;20(7).
118. Aasen T, Leithe E, Graham S v., Kameritsch P, Mayán MD, Mesnil M, et al. Connexins in cancer: bridging the gap to the clinic. Oncogene. 2019 Jun 27;38(23).

119. Zefferino, Piccoli, Gioia, Capitanio, Conese. Gap Junction Intercellular Communication in the Carcinogenesis Hallmarks: Is This a Phenomenon or Epiphenomenon? Cells. 2019 Aug 14;8(8).
120. Asencio-Barría C, Defamie N, Sáez JC, Mesnil M, Godoy AS. Direct Intercellular Communications and Cancer: A Snapshot of the Biological Roles of Connexins in Prostate Cancer. Cancers. 2019 Sep 14;11(9).
121. Umhauer S, Ruch RJ, Fanning J. Gap junctional intercellular communication and connexin 43 expression in ovarian carcinoma. American Journal of Obstetrics and Gynecology. 2000 May;182(5).
122. Toler CR, Taylor DD, Gercel-Taylor C. Loss of communication in ovarian cancer. American Journal of Obstetrics and Gynecology. 2006 May;194(5).
123. Liang B, Peng P, Chen S, Li L, Zhang M, Cao D, et al. Characterization and proteomic analysis of ovarian cancer-derived exosomes. Journal of Proteomics. 2013 Mar;80.
124. Lou E. A Ticket to Ride: The Implications of Direct Intercellular Communication via Tunneling Nanotubes in Peritoneal and Other Invasive Malignancies. Frontiers in Oncology. 2020 Nov 26;10.
125. Caliari SR, Burdick JA. A practical guide to hydrogels for cell culture. Nature Methods. 2016 May 28;13(5).
126. Yao D, Dai C, Peng S. Mechanism of the Mesenchymal-Epithelial Transition and Its Relationship with Metastatic Tumor Formation. Molecular Cancer Research. 2011 Dec 1;9(12).
127. Yi B-R, Kim T-H, Kim Y-S, Choi K-C. Alteration of epithelial-mesenchymal transition markers in human normal ovaries and neoplastic ovarian cancers. International Journal of Oncology. 2015 Jan;46(1).
128. Chen Z, Wang Y, Liu W, Zhao G, Lee S, Balogh A, et al. Doxycycline Inducible Kruppel-Like Factor 4 Lentiviral Vector Mediates Mesenchymal to Epithelial Transition in Ovarian Cancer Cells. PLoS ONE. 2014 Aug 19;9(8).
129. McLean K, Gong Y, Choi Y, Deng N, Yang K, Bai S, et al. Human ovarian carcinoma–associated mesenchymal stem cells regulate cancer stem cells and tumorigenesis via altered BMP production. Journal of Clinical Investigation. 2011 Aug 1;121(8).
130. Tiwari A, Hadley JA, Ramachandran R. Characterization of ascites-derived aldehyde dehydrogenase–positive ovarian cancer stem cells isolated from Leghorn chickens. Poultry Science. 2020 Apr;99(4).
131. Lee S, Yang Y, Fishman D, Banaszak Holl MM, Hong S. Epithelial–Mesenchymal Transition Enhances Nanoscale Actin Filament Dynamics of Ovarian Cancer Cells. The Journal of Physical Chemistry B. 2013 Aug 8;117(31).
132. Schiewek J, Schumacher U, Lange T, Joosse SA, Wikman H, Pantel K, et al. Clinical relevance of cytoskeleton associated proteins for ovarian cancer. Journal of Cancer Research and Clinical Oncology. 2018 Nov 9;144(11).
133. Chauhan SC, Vannatta K, Ebeling MC, Vinayek N, Watanabe A, Pandey KK, et al. Expression and functions of transmembrane mucin MUC13 in ovarian cancer. Cancer Research. 2009 Feb 1;69(3):765–74.

134. Jalal S, Shi S, Acharya V, Huang RYJ, Viasnoff V, Bershadsky AD, et al. Actin cytoskeleton self-organization in single epithelial cells and fibroblasts under isotropic confinement. Journal of Cell Science. 2019 Mar 1;132(5).
135. Rohnalter V, Roth K, Finkernagel F, Adhikary T, Obert J, Dorzweiler K, et al. A multi-stage process including transient polyploidization and EMT precedes the emergence of chemoresistent ovarian carcinoma cells with a dedifferentiated and pro-inflammatory secretory phenotype. Oncotarget. 2015 Nov 24;6(37).
136. Urruticoechea A, Smith IE, Dowsett M. Proliferation Marker Ki-67 in Early Breast Cancer. Journal of Clinical Oncology. 2005 Oct 1;23(28).
137. Sobecki M, Mrouj K, Colinge J, Gerbe F, Jay P, Krasinska L, et al. Cell-Cycle Regulation Accounts for Variability in Ki-67 Expression Levels. Cancer Research. 2017 May 15;77(10).
138. Battista MJ, Mantai N, Sicking I, Cotarelo C, Weyer V, Lebrecht A, et al. Ki-67 as an independent prognostic factor in an unselected cohort of patients with ovarian cancer: Results of an explorative, retrospective study. Oncology Reports. 2014 May;31(5).
139. Rahmanzadeh R, Rai P, Celli JP, Rizvi I, Baron-Luhr B, Gerdes J, et al. Ki-67 as a Molecular Target for Therapy in an In vitro Three-Dimensional Model for Ovarian Cancer. Cancer Research. 2010 Nov 15;70(22).
140. Akbarzadeh M, Movassaghpour AA, Ghanbari H, Kheirandish M, Fathi Maroufi N, Rahbarghazi R, et al. The potential therapeutic effect of melatonin on human ovarian cancer by inhibition of invasion and migration of cancer stem cells. Scientific Reports. 2017 Dec 6;7(1).
141. Chen M, Yao S, Cao Q, Xia M, Liu J, He M. The prognostic value of Ki67 in ovarian high-grade serous carcinoma: an 11-year cohort study of Chinese patients. Oncotarget. 2017 Dec 8;8(64).
142. Mahadevappa A. Diagnostic and Prognostic Significance of Ki-67 Immunohistochemical Expression in Surface Epithelial Ovarian Carcinoma. JOURNAL OF CLINICAL AND DIAGNOSTIC RESEARCH. 2017;
143. Vital-Reyes V, Rodríguez-Burford C, Chhieng DC, Oelschlager DK, Reyes-Fuentes A, Barnes M, et al. Celecoxib Inhibits Cellular Growth, Decreases Ki-67 Expression and Modifies Apoptosis in Ovarian Cancer Cell Lines. Archives of Medical Research. 2006 Aug;37(6).
144. Niu N, Zhang J, Zhang N, Mercado-Uribe I, Tao F, Han Z, et al. Linking genomic reorganization to tumor initiation via the giant cell cycle. Oncogenesis. 2016 Dec 19;5(12).
145. Niu N, Mercado-Uribe I, Liu J. Dedifferentiation into blastomere-like cancer stem cells via formation of polyploid giant cancer cells. Oncogene. 2017 Aug 24;36(34).
146. Zhang S, Mercado-Uribe I, Xing Z, Sun B, Kuang J, Liu J. Generation of cancer stem-like cells through the formation of polyploid giant cancer cells. Oncogene. 2014 Jan 2;33(1).
147. Klymenko Y, Kim O, Stack M. Complex Determinants of Epithelial: Mesenchymal Phenotypic Plasticity in Ovarian Cancer. Cancers. 2017 Aug 9;9(12).

148. Pakuła M, Uruski P, Niklas A, Woźniak A, Szpurek D, Tykarski A, et al. A Unique Pattern of Mesothelial-Mesenchymal Transition Induced in the Normal Peritoneal Mesothelium by High-Grade Serous Ovarian Cancer. Cancers. 2019 May 13;11(5).
149. Kalamegam G, Sait KHW, Ahmed F, Kadam R, Pushparaj PN, Anfinan N, et al. Human Wharton's Jelly Stem Cell (hWJSC) Extracts Inhibit Ovarian Cancer Cell Lines OVCAR3 and SKOV3 in vitro by Inducing Cell Cycle Arrest and Apoptosis. Frontiers in Oncology. 2018 Dec 7;8.
150. Rosales-Leal JI, Rodríguez-Valverde MA, Mazzaglia G,Ramón-Torregrosa PJ, Díaz-Rodríguez L, García-Martínez O, et al. Effect of roughness, wettability and morphology of engineered titanium surfaces on osteoblast-like cell adhesion. Colloids and Surfaces A: Physicochemical and Engineering Aspects. 2010 Aug;365(1–3).
151. Jain G, Ford AJ, Rajagopalan P. Opposing Rigidity-Protein Gradients Reverse Fibroblast Durotaxis. ACS Biomaterials Science & Engineering. 2015 Aug 10;1(8).
152. Lane D, Matte I, Garde-Granger P, Laplante C, Carignan A, Rancourt C, et al. Inflammation-regulating factors in ascites as predictive biomarkers of drug resistance and progression-free survival in serous epithelial ovarian cancers. BMC Cancer. 2015 Dec 1;15(1).
153. Gilmore AP. Anoikis. Cell Death & Differentiation. 2005 Nov 25;12(S2).
154. Kim Y-N, Koo KH, Sung JY, Yun U-J, Kim H. Anoikis Resistance: An Essential Prerequisite for Tumor Metastasis. International Journal of Cell Biology. 2012;2012.
155. Liu W, Watabe K. Apoptosis, Anoikis, and Senescence. In: Lyden D, Welch DR, Psaila B, editors. Cancer Metastasis. Cambridge: Cambridge University Press;
156. Nakayama K, Nakayama N, Katagiri H, Miyazaki K. Mechanisms of Ovarian Cancer Metastasis: Biochemical Pathways. International Journal of Molecular Sciences. 2012 Sep 18;13(12).
157. Paszek MJ, Zahir N, Johnson KR, Lakins JN, Rozenberg GI, Gefen A, et al. Tensional homeostasis and the malignant phenotype. Cancer Cell. 2005 Sep;8(3).
158. Gkretsi V, Stylianopoulos T. Cell Adhesion and Matrix Stiffness: Coordinating Cancer Cell Invasion and Metastasis. Frontiers in Oncology. 2018 May 4;8.
159. Riedl A, Schlederer M, Pudelko K, Stadler M, Walter S, Unterleuthner D, et al. Comparison of cancer cells in 2D vs 3D culture reveals differences in AKT-mTOR-S6K signaling and drug responses. Journal of Cell Science. 2017;130(1):203–18.
160. Kalamegam G, Sait KHW, Ahmed F, Kadam R, Pushparaj PN, Anfinan N, et al. Human Wharton's Jelly Stem Cell (hWJSC) Extracts Inhibit Ovarian Cancer Cell Lines OVCAR3 and SKOV3 in vitro by Inducing Cell Cycle Arrest and Apoptosis. Frontiers in Oncology. 2018 Dec 7;8.
161. Sallum LF, Andrade L, Ramalho S, Ferracini AC, de Andrade Natal R, Brito ABC, et al. WT1, p53 and p16 expression in the diagnosis of low- and high-

grade serous ovarian carcinomas and their relation to prognosis. Oncotarget. 2018 Mar 23;9(22).
162. Giannakouros P, Comamala M, Matte I, Rancourt C, Piché A. Original Article MUC16 mucin (CA125) regulates the formation of multicellular aggregates by altering β-catenin signaling [Internet]. Vol. 5, Am J Cancer Res. 2015. Available from: www.ajcr.us/
163. Dadgar N, Gonzalez-Suarez AM, Fattahi P, Hou X, Weroha JS, Gaspar-Maia A, et al. A microfluidic platform for cultivating ovarian cancer spheroids and testing their responses to chemotherapies. Microsystems & Nanoengineering. 2020 Dec 19;6(1).
164. Raghavan S, Ward MR, Rowley KR, Wold RM, Takayama S, Buckanovich RJ, et al. Formation of stable small cell number three-dimensional ovarian cancer spheroids using hanging drop arrays for preclinical drug sensitivity assays. Gynecologic Oncology. 2015 Jul;138(1).
165. Wong C, Vosburgh E, Levine AJ, Cong L, Xu EY. Human Neuroendocrine Tumor Cell Lines as a Three-Dimensional Model for the Study of Human Neuroendocrine Tumor Therapy. Journal of Visualized Experiments. 2012 Aug 14;(66).
166. Govindarajan M, Wohlmuth C, Waas M, Bernardini MQ, Kislinger T. High-throughput approaches for precision medicine in high-grade serous ovarian cancer. Journal of Hematology & Oncology. 2020 Dec 9;13(1).
167. Tudrej P, Olbryt M, Zembala-Nożyńska E, Kujawa K, Cortez A, Fiszer-Kierzkowska A, et al. Establishment and Characterization of the Novel High-Grade Serous Ovarian Cancer Cell Line OVPA8. International Journal of Molecular Sciences. 2018 Jul 17;19(7).
168. Pakuła M, Uruski P, Niklas A, Woźniak A, Szpurek D, Tykarski A, et al. A Unique Pattern of Mesothelial-Mesenchymal Transition Induced in the Normal Peritoneal Mesothelium by High-Grade Serous Ovarian Cancer. Cancers. 2019 May 13;11(5).
169. Hallas-Potts A, Dawson JC, Herrington CS. Ovarian cancer cell lines derived from non-serous carcinomas migrate and invade more aggressively than those derived from high-grade serous carcinomas. Scientific Reports. 2019 Dec 2;9(1).
170. Dietrich CS, Greenberg VL, DeSimone CP, Modesitt SC, van Nagell JR, Craven R, et al. Suberoylanilide hydroxamic acid (SAHA) potentiates paclitaxel-induced apoptosis in ovarian cancer cell lines. Gynecologic Oncology. 2010 Jan;116(1).
171. Kalanxhi E, Risberg K, Barua IS, Dueland S, Waagene S, Andersen SN, et al. Induction of Apoptosis in Intestinal Toxicity to a Histone Deacetylase Inhibitor in a Phase I Study with Pelvic Radiotherapy. Cancer Research and Treatment. 2017 Apr 15;49(2).
172. Lujambio A, Esteller M. How epigenetics can explain human metastasis: A new role for microRNAs. Cell Cycle. 2009 Feb 28;8(3).

173. Wu X, Zhuang Y, Hong C, Chen J, You Y, Zhang F, et al. Clinical importance and therapeutic implication of E-cadherin gene methylation in human ovarian cancer. Medical Oncology. 2014 Aug 29;31(8).
174. Herbein G, Nehme Z. Polyploid Giant Cancer Cells, a Hallmark of Oncoviruses and a New Therapeutic Challenge. Frontiers in Oncology. 2020 Oct 14;10.
175. Zhang L, Ding P, Lv H, Zhang D, Liu G, Yang Z, et al. Number of Polyploid Giant Cancer Cells and Expression of EZH2 Are Associated with VM Formation and Tumor Grade in Human Ovarian Tumor. BioMed Research International. 2014;2014.
176. Fei F, Zhang M, Li B, Zhao L, Wang H, Liu L, et al. Formation of Polyploid Giant Cancer Cells Involves in the Prognostic Value of Neoadjuvant Chemoradiation in Locally Advanced Rectal Cancer. Journal of Oncology. 2019 Aug 29;2019.
177. Roles of Polyploid/Multinucleated Giant Cancer Cells in Metastasis and Disease Relapse Following Anticancer Treatment. Cancers. 2018 Apr 15;10(4).
178. Maison C, Bailly D, Peters AHFM, Quivy J-P, Roche D, Taddei A, et al. Higher-order structure in pericentric heterochromatin involves a distinct pattern of histone modification and an RNA component. Nature Genetics. 2002 Mar 19;30(3).
179. Klymenko Y, Johnson J, Bos B, Lombard R, Campbell L, Loughran E, et al. Heterogeneous Cadherin Expression and Multicellular Aggregate Dynamics in Ovarian Cancer Dissemination. Neoplasia. 2017 Jul;19(7).
180. Teng L, Peng S, Guo H, Liang H, Xu Z, Su Y, et al. Conditioned media from human ovarian cancer endothelial progenitor cells induces ovarian cancer cell migration by activating epithelial-to-mesenchymal transition. Cancer Gene Therapy. 2015 Nov 23;22(11).
181. Campo L, Zhang C, Breuer E-K. EMT-Inducing Molecular Factors in Gynecological Cancers. BioMed Research International. 2015;2015.